# THE ROLE OF PHYSICAL MODELING IN OFFSHORE GEOTECHNICAL ENGINEERING

Edward C. Clukey, GeoMaxEd, The Woodlands, TX, USA, 832-875-0596, ed.clukey@outlook.com

## ABSTRACT

Physical model testing is an important part of offshore geotechnical engineering and has been used to verify foundation designs and provide important information for addressing new and challenging problems. Due to the loads and dimensions of many offshore geotechnical problems, it is often not possible to simulate prototype conditions; innovative approaches are then required to develop creative cost-effective solutions. Physical model testing, however, does not exist alone and ideally should be augmented by numerical modeling and field results. Numerical modeling can be calibrated to model tests and then used to perform sensitivity assessments of geotechnical and foundation data. Both types of modeling are complementary and when used appropriately can provide robust solutions to problems. The paper presents results from physical model test programs investigating the following offshore geotechnical problems: 1) wave-seafloor interaction, 2) debris flow impact on pipelines, 3) behavior of suction caissons in clays and sands, 4) fatigue issues for conductors and steel catenary risers, and 5) the response of steel pile jackets and subsea manifolds/wells to earthquake induced ground motions. The tests were performed under a variety of testing conditions, including 1g models, centrifuge models, foundation element modelling and fully coupled foundation-structure modelling. Some were small scale tests which did not match similitude scaling conditions while others were able to match many scaling relationships. All tests, however, provided important insights and advancements to the problems they addressed.

**Keywords: model testing, centrifuge, fatigue, suction caissons, earthquakes, wave loading**

## INTRODUCTION

I was first introduced to offshore geotechnical engineering by Professor Armand Silva in 1973. At that time, Professor Silva and others were beginning to work with marine geologists to characterize deep sea sediments for a variety of purposes including the potential offshore burial of nuclear waste material. As work in this area advanced with samples collected with largely standard or Giant Piston Cores, other work in shallower water depths related to foundation designs for offshore platforms had been progressed for over 15 years by McClelland engineers. It was obvious that Mr. McClelland and McClelland Engineers were the leaders in this offshore geotechnical development, not only for advancing sampling techniques and site characterization, but also for the development of offshore industry practices.

In 1983, I accepted an offer for McClelland Engineers in their Ventura, CA office. By that time, McClelland Engineers had become a fully integrated worldwide offshore company with technical expertise well beyond the purview of traditional geotechnical engineering. The evolution of integrated offshore studies had begun requiring expertise and knowledge from a variety of disciplines.

For a brief one-month period in 1984, I was asked to work in the Houston office on several Gulf of Mexico (GoM) projects and had the opportunity to introduce myself to Mr. McClelland. From the limited time I was able to spend with him, I sensed his profound interest in the challenges we were facing in California and in my own development as an engineer. Although I could have listened the entire time to his perspectives on offshore geotechnical engineering, he was just as interested in me and my thoughts. The meeting was relatively short, but I did come away with a sense that he was a very practical man dedicated to the engineering profession and its people.

Similar to Don Murff's introductory comments in the 1st McClelland Lecture, I feel that, although I have picked a topic somewhat different from the major focus of McClelland Engineers, he would be pleased that I have chosen physical modeling as the topic of this lecture and would be just as interested as he was during our 1984 conversation.

My predecessors for this lecture have, like Mr. McClelland, set a high standard of achievement. The first two lecturers (Don Murff and Mark Randolph) both focused on the value of analytical solutions in practice. These lectures were then followed by the comprehensive 3rd McClelland lecture by Knut Andersen which addressed the challenge of establishing cyclic parameters for design. The most recent lecture by Alan Young on integrated studies perhaps mirrored a perspective that was closest to Mr. McClelland's own technical legacy.

Despite the very excellent and comprehensive nature of all these previous lectures we are fortunate to be in a field that provides ever increasing opportunities to explore different approaches to problems. The topic I have chosen is the role physical modeling has in addressing offshore geotechnical problems. Of course, even a cursory review of this topic reveals vast amounts of information. A conference in Perth on Physical Modeling in Geotechnics (2014) attracted almost 200 papers with many addressing offshore related problems. The advent of centrifuge testing for over 40 years in the offshore geotechnical community has added substantially to the information database with 8 international conferences. Papers by Murff (1996) and Gaudin et al. (2010) summarize a variety of offshore studies using the centrifuge approach. Therefore, the lecture does not attempt to capture or review even a small fraction of this information, but rather will attempt to show for a range of offshore related problems how physical model testing has provided key insights to problem solving and design.

The examples covered include: 1) wave-seafloor interaction, 2) impact of debris flows on pipelines, 3) suction caisson technology, 4) fatigue related issues for conductors and Steel Catenary Risers (SCRs), and 5) offshore earthquake engineering. Prior to these examples, however, some important considerations and the author's own experience and views regarding physical model testing are presented.

## PHYSICAL MODEL TESTING-OVERVIEW

There is a wide range of physical modeling techniques used in geotechnical engineering, from proof tests of actual foundations to small scale laboratory tests. These various tests can be performed to verify a design approach or to achieve a more fundamental understanding of the mechanics for a problem.

In the case of a design proof test a full understanding of the foundation mechanics is not necessarily required. In these types of tests instrumentation is often minimal and the tests are often performed to verify a minimum capacity or maximum displacement levels. These types of tests are less frequent for offshore applications where the foundation sizes and loads plus high costs often preclude their usage. High instrument failure rates are also an issue in harsh offshore environments. These programs must also include sensors to determine the loads which are often substantially less than the more extreme loads required for design. An exception to this is fatigue loads where the most damaging conditions are those associated with smaller-sized events. Despite all these challenges, field measurements provide valuable information that serve as critical benchmarks for results derived by other methods.

Physical modeling, of course, does not exist in a vacuum and often is performed in association with analytical or numerical modeling. Much greater confidence is achieved when reasonable agreement occurs between these different approaches. However, a wide range of analytical and numerical approaches are available. On one end, full 3-dimensional finite element models are now available that can incorporate very advanced constitutive models and accommodate

large displacements (Templeton 2002; 2012 ;2019). Even with these techniques, however, uncertainties exist such as the foundation performance along interfaces (e.g. soil gapping) or for cases with significant cyclic loading. Although several commercial software packages are available which address these issues, the level of expertise required to reliably implement the methods is often quite high. If these techniques are used, even with experienced analysts, appropriate calibration through field data or physical model tests is still important.

When less sophisticated analytical approaches are used (usually the case for design) several limitations should be noted. First, the methods often may have approximations that make them inapplicable to a broader range of problems. They may also have been calibrated to physical model tests (or field data) that require significant extrapolation to the problems of interest.

## *Types of Physical Model Tests*

Physical model tests can be differentiated into the following types:

1. Segment tests: where a foundation component or a segment of the foundation system (e.g. pile, anchor, pipeline, conductor, riser, etc.) are tested.
2. Sectional tests: where the entire foundation and some of the structural system beyond that in contact with the soil is considered.
3. System tests: where the entire foundation and structural system are tested together.

The first type (segment) has been quite helpful recently for determining soil-pipe interaction for pipelines undergoing buckling from thermal expansion and pipeline walking as well as determining appropriate soil stiffness values for Steel Catenary Riser (SCR) fatigue assessments (SAFEBUCK 2015; Bridge et al. 2004; Bridge 2005). In this type of testing a short section of pipe, usually on the order of 0.5 m to 1.0 m long is tested by moving the pipe in either the axial, lateral or vertical directions. Tests of this nature, however, do not provide information regarding the interactions along the pipe.

The second type of testing is perhaps the most common type of physical model testing. Examples of this type of testing would include pile load tests, conductor fatigue tests, shallow footing tests or some more recent tests on SCRs where a portion of the SCR through the touchdown region is tested. Since these tests only comprise a portion of the overall foundation-structural system, assumptions (e.g pinned versus fixed connections) are required concerning the interaction between the foundation and structure.

The third type of testing includes the structure in the physical modeling. Although this type of testing likely provides the most information it is done far less frequently because: 1) the size of the model becomes physically too large for many testing facilities, 2) added collaboration required between geotechnical and other engineering disciplines and 3) cost.

It should be noted, that in lieu of performing the third type of testing, the results obtained from the previous two test types are often implemented into analytical or numerical models to determine the overall system response. This may not always be a sound procedure depending on the influence of the structural component on the physical modeling results such as potential impacts on failure mechanisms and frequency/resonance considerations for dynamic problems.

## *Scaling Relationships*

In the study of any engineering problem it is important to understand the basic parameters that most impact the problem. A formalized approach to assessing these parameters is through dimensional analysis using Buckingham Pi theory (Buckingham 1914). A very good example of how Buckingham Pi can be applied to develop the well-known Reynolds number

can be found at: https://www.youtube.com/watch?v=J7khnExq9aE. Experienced engineers can often determine many of the dimensionless variables for a problem without relying on the theory, but its usage is highly recommended.

In geotechnical problems with an increasing shear strength profile with depth, the normalization of the undrained shear strength is an important parameter for consideration. For normally consolidated soils this normalization is simply:

$$S_u/p' \quad [1]$$

Where $S_u$ is the undrained shear strength and $p'$ is the overburden stress. For the case where the soil is overconsolidated, the relationship becomes:

$$S_u/p' = A\ OCR^B \quad [2]$$

Where $A$ and $B$ are material coefficients and $OCR$ is the overconsolidation ratio. Therefore, for clay soils the strength of the material is highly dependent on the effective overburden stress. The overburden is, of course. equal to:

$$(\rho_{soil} - \rho_{water})gz \quad [3]$$

Where $\rho_{soil}$ is the soil density, $\rho_{water}$ is the water density, $g$ is the gravitational acceleration and $z$ is the depth. For geotechnical problems, particularly with offshore deposits where we frequently find normally to slightly overconsolidated clay soils, the strength and behavior of the material and the foundation performance is highly dependent on the overburden or body forces of the material and needs to be considered in physical model tests.

However, even with this constraint, for some problems smaller sized model tests can satisfy similitude for some conditions. For instance, for a square footing at the seafloor Buckingham Pi theory would indicate that similitude is achieved for the vertical capacity if the dimensionless parameter

$$F_v/(B^2 S_u) \quad [4]$$

Where $F_v$ is the vertical failure load, $B$ is the foundation width and $S_u$ is the undrained shear strength. Similitude is satisfied if the shear strength is the same for both the model and prototype. For this case the prototype failure load could be determined by multiplying the load measured in the model by $N^2$ where $NB_m = B_p$ and the subscripts $m$ and $p$ refer to the model and prototype. If the shear strength for both model and prototype were to increase proportionally with depth, as is frequently the case for offshore soils, then the dimensional relationship would suggest that the relationship between the model and prototype failure load is $N^3$.

For a shallow embedded foundation, however, there are two additional dimensionless factors:

$$d/B \quad [5]$$

and

$$S_u/(B\gamma) \quad [6]$$

Where $d$ is the embedment depth, must be satisfied for proper similitude. The first factor $(d/B)$ is easily satisfied by scaling both the foundation width and embedment depth with the same scaling factor. The second factor, $S_u/(B\gamma)$, is the result of the unbalanced soil weights inside and outside the foundation footprint and is more difficult to model with small-scale tests.

Similitude for this last condition could potentially be achieved for this dimensionless factor by the use of centrifuge testing to achieve the prototype shear strength, unit weight and prototype dimensions. Centrifuge scaling relationships will be discussed more later in the paper but, as discussed above, the shear strength is a function of the effective overburden stress which is $\gamma' z$ or $(\rho_{soil} - \rho_{water})gz$. Therefore, if the model is $N$ times smaller than the prototype the submerged unit weight $(\gamma')$, shear strength $(S_u)$, and model dimension can all be scaled properly if the model is tested at a $g$ level equal to the ratio of the prototype/model sizes.

It should be noted that for side friction on a pile or suction caisson smaller sized model tests can be properly scaled by $N^3$ if the shear strength gradient in the model tests is the same as the prototype and the side friction coefficient $(\alpha)$ is not dependent on stress level. Recent work on the axial resistance of pipelines resting on the seafloor (Bruton et al. 2009; White et al. 2017), however, has shown (Fig. 1) that the limiting friction along a pipe will vary significantly at low stress levels.

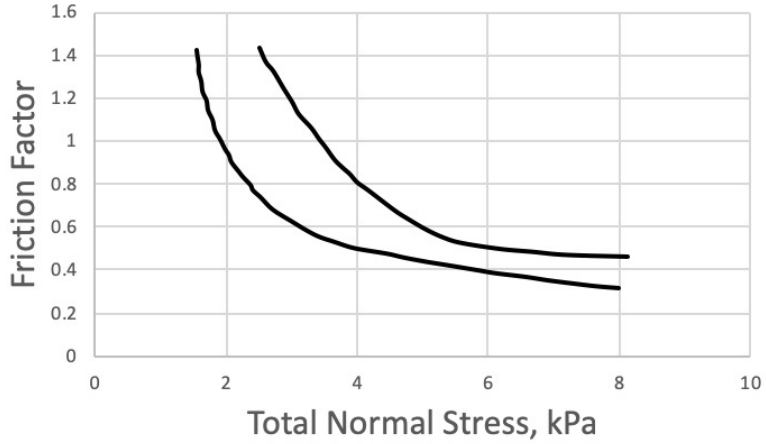


**Fig. 1. Friction coefficient versus stress level for pipe on the seafloor (modified from Bruton et al. 2009)**

As shown on this Fig. 1, the axial friction factor (axial force/pipe weight) is not uniform and continues to decrease up to total stresses of about 7 to 8 kPa. For typical soils (e.g. GoM) with unit weights in the upper few meters of 5 to 6 kN/m$^3$, the data suggests that the stress range with non-uniform friction would be equivalent to about 1.5 m of overburden. Even though the stress conditions around a pipe on the seafloor and a pile are different, these results do suggest the possible risks of extrapolating pile test results only a few meters long to 100 m or more long offshore piles.

LeBlanc et al. (2010) also note the well-known stress level effect for cohesionless soils where dilation depends on both the relative density and stress level.

Considering the scaling relationships for limit state conditions for lateral loads on piles (or suction caissons) in clays, Murff and Hamilton (1993) have identified three contributors to the lateral capacity. These are: a) a wedge failure toward the top of the pile, b) a flow around zone starting at the bottom of the wedge failure and extending to the bottom of the pile and c) a 'scoop' mechanism at the bottom of the pile. The wedge failure will have, assuming no gapping at the trailing side of the pile, an active and passive component which will both be dependent on the body forces or unit weight of the soil. This component of the failure mechanism would scale correctly if the weight of the active and passive wedges were equal since the two would cancel with the passive wedge moving upwards and the active wedge downwards. However, the passive and active weights of these wedges are not necessarily equal with the dissimilarity exacerbated if gapping occurs on the back side of the caisson.

Suctions caissons in uplift can also be properly simulated with small tests, assuming no difference in the interface friction, the same shear strength gradients and the same height of the soil plug inside and outside the caisson. Therefore, the dimensionless factor, $S_u/(B\gamma)$, discussed above may not negatively influence the scaling.

## *Centrifuge Scaling*

Based on Buckingham Pi scaling, relationships between the models and prototypes can be derived for tests at higher $g$-levels. Garnier et al. (2007) provide a comprehensive discussion of these relationships. Fundamentally centrifuge testing elevates the $g$-level in the model test to simulate proper body forces. Therefore, the model characteristic dimensions are reduced by the same proportion as the $g$-level. Length dimensions $(L)$ in the model then scale with the $g$-level to simulate prototype dimensions

$$(L_m N) = L_p \quad [7]$$

Where $N$ is the elevated g-level in the centrifuge. Therefore, a 1 m model accelerated at $10g$ in the centrifuge models a 10-m long prototype condition. Some of the more frequently encountered scaling relationships are shown on Table 1.

**Table 1. Scaling factors in the centrifuge for test performed at *Ng***

| Parameter | Scale Factor |
|---|---|
| Length | $L_m N = L_p$ |
| Stress | $\sigma_m = \sigma_p$ |
| Density | $\rho_m = \rho_p$ |
| Time - Pore Pressure Diffusion | $T_m N^2 = T_p$ |
| Time - Acceleration | $T_m N = T_p$ |
| Force | $F_m N^2 = F_p$ |
| Strain | $\varepsilon_m = \varepsilon_p$ |
| Mass | $M_m N^3 = M_p$ |

It should be noted that all the variables listed above would be measured in the centrifuge when the centrifuge is accelerating at $Ng$. For example, if a load cell measured a force in the centrifuge at $Ng$, this measured value would then be scaled upwards by $N^2$ to represent the prototype force. Stresses scale equally due to the $N^2$ factor on force and area. A practical consequence of the $N^2$ relationship for the force is that large actuators are not required to reach prototype load conditions.

An important scaling factor involves the time required for pore pressure diffusion or consolidation. The dimensionless time factor for consolidation is the familiar

$$T = \frac{c_v t}{H^2} \quad [8]$$

Where $c_v$ is the coefficient of consolidation, $t$ is time and $H$ is the characteristic length to a free drainage surface. Through dimensional analysis it can be shown that $c_v$ in the model and the centrifuge are the same (assuming the same soil is used and has the same void ratio).

Therefore, for this dimensionless time factor to be the same for both the model and prototype the time must scale as $N^2$ since the length dimensions $(H)$ scale with $N$ and is squared in the denominator in Eq. 8. The resulting scaling relationship shown in Table 1 has two significant practical applications. First the equivalent consolidation time in the centrifuge to prepare a sample for testing is much faster in the centrifuge. Test specimens can then be prepared in hours to a few days. For example, 1 day of consolidation time in a centrifuge test performed at $100g$ would result in 10,000 days (about 27 years) of consolidation time for the prototype case. However, this faster diffusion rate also means that to maintain undrained conditions during loading, tests should be performed at high rates of loading. High rates of loading can also induce rate effects that could result in higher shear strengths than those typically measured at slower rates. The selected shear strength used to analyze centrifuge data should be consistent with methods used to determine the shear strength and the loading rates used in the centrifuge tests.

Finally, the scaling for time-acceleration listed in Table 1 refers to acceleration levels incurred from external loadings. This scaling relationship is usually of most concern for earthquake problems, but it would be relevant for other problems where inertial effects are important, such as impact loads or gravity penetrating (torpedo) anchors.

From Buckingham Pi it can be shown that to achieve prototype acceleration levels and properly model inertial effects the acceleration in the model must be $N$ times greater or:

$$a_m = N a_p \quad [9]$$

From the definition of acceleration in both the model and prototype it can be further shown that the time in the model of the applied acceleration needs to be reduced, as shown on Table 1, by $N$ or:

$$T_m = T_p / N \quad [10]$$

To satisfy similitude between model and prototype then requires shake tables capable of very large accelerations applied over a short time period (e.g. a $1g$ acceleration at 1 Hz needs to be modeled at a centrifuge acceleration of $100g$ as a $100g$ shake table acceleration at 100 Hz).

## *Sample Preparation*

Model tests can be performed by either installing the model foundation into the *in-situ* material or by remolding and then reconstituting the soil in the laboratory. Ideally, for clays, the soil should return to the same *in-situ* shear strength and OCR as the prototype. Although it could be argued that achieving the same shear strength gradient without matching the OCR profile could result in similar failure states there are a number of potentially significantly differences. For example, the soil stiffness and displacements would likely be different and corresponding differences in soil anisotropy could impact the foundation capacity. Therefore, the sample preparation should strive to match both the shear strength and OCR profiles.

Problems with reconstituted samples can possibly occur for highly structured or sensitive clays with metastable structure. Jeanjean (2006) provided some insight on clay structure issues by examining extraction pull-out data and set-up times for suction caissons used to anchor Mobile Offshore Drilling Units (MODUs). Based on pullout times from about 0.02 to over 1,000 days he was able to match the field results (Fig. 2) with either a thixotropy (Andersen et al. 2003) or pore pressure dissipation-consolidation model (Andersen and Jostad 2002).

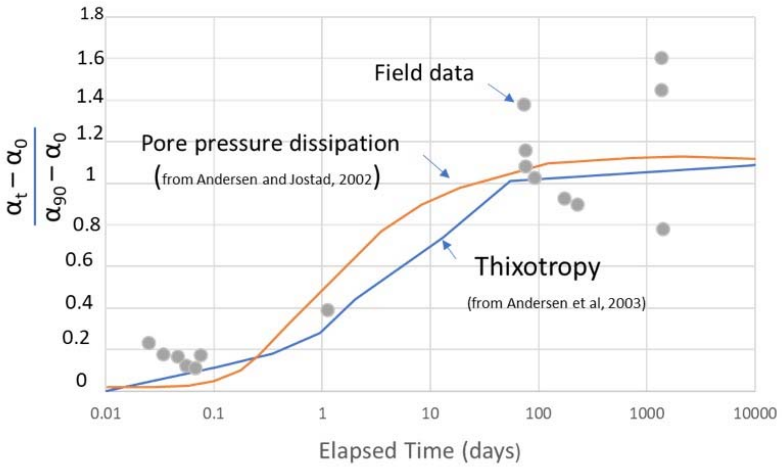


**Fig. 2. Relationships between pore pressure dissipation and thixotropy versus field data (modified from Jeanjean 2006)**

Thixotropy is defined as the increase in shear strength with time at a constant soil density. In Fig. 2, $\alpha_0$ is the average side friction normalized by the undrained shear strength after installation; frequently assumed to be

$$1/S_t \qquad [11]$$

Where $S_t$ is the soil sensitivity. For GoM clays, $\alpha_0$ frequently ranges from 0.25 to 0.33. The $\alpha_t$ and $\alpha_{90}$ values are at any elapsed time, $t$, and at 90% of the final estimated set-up value. In this example $\alpha_{90}$ was 0.75. The results suggest that for very small elapsed times (<0.1 days) the combination of consolidation and thixotropy models provide a good match to the measured data. Beyond 1 day either model appears to provide reasonably good predictions. However, beyond 1 day the combination of the model results would significantly overestimate the measured values.

Therefore, based on these results it appears that normal consolidation processes alone could account for the increase in friction along the side of the caisson, except in the first few hours after installation, even though much of the clay structure next to the side walls would have been lost initially. It is also the author's opinion that the consolidation process is fundamentally better understood. Thixotropy studies are also usually based on laboratory studies with different conditions versus the field case. Mitchell (1993) states that the extent to which thixotropic hardening can account for the sensitivity of the soil is impossible to determine from laboratory tests, because the conditions in the field are much different than conditions in the lab wherethe tests are typically performed at very low effective stresses. The efficacy of the consolidation process is further supported by many model tests which have been found to replicate expected results.

Possible exceptions where remolded-reconstituted soils may not accurately replicate field conditions are soils with metastable structures or cemented soils such as those that have high carbonate content. For other more frequently encountered soils it appears that remolded-reconstituted samples will produce representative results.

## *Instrumentation and Testing Guidelines*

The effectiveness of any model test program depends on numerous factors such as those discussed above. Beyond these factors: a) the proper calibration of instruments in the conditions expected during the testing, b) the type of load application - load versus displacement control, and c) the proximity of boundary constraints will all impact the results.

Some instruments such as LVDTs or lasers have limited negative impact since these are not directly integrated into the soil. Strain gauges, on the other hand, can add weight and stiffness to the model tests, especially when protective water-proof coating is required.

Fiber optic techniques can provide an alternative to strain gauging. They can be particularly useful in centrifuge testing performed at high g-levels when the reduced model size makes strain gauges difficult to install. Instruments such as pore pressures transducers, stress cells and accelerometers installed in the soil all impact the results based on their weight and stiffness and their potential to change the stress conditions within the soil. They should be properly calibrated to determine their level of impact. Instrument miniaturization will reduce the impact. Over instrumentation in the soil mass, however, should be avoided. Techniques such as Particle Image Velocimetry (White et al. 2003; 2005) provide a means for assessing flow patterns and failure mechanisms with minimal impact on the soil mass and response.

Ultimately all experimental results will have some degree of error and uncertainty. The ability of individual investigators to reproduce their results is the first step in reducing this uncertainty. Results obtained from multiple investigations (and investigators) helps eliminate bias and improves confidence in the results.

Finally, the opportunity to perform a series of tests enhances the ability to isolate key model parameters. Relatively simple objectives for the initial tests provide important benchmarks for future tests and are more likely to produce more immediate useful data to justify additional testing. More complex initial testing may have a upside potential, but they will have a greater risk of failure. Successful initial tests will enhance the learning process for the investigator and provide confidence for pursuing more advanced tests.

## WAVE-SEAFLOOR INTERACTION

### *Overview*

The interaction of ocean waves with the seafloor has been of interest to the offshore geotechnical community for many years. This interest was initiated by the failure of two steel jacket platforms in the South Pass region of the GoM in 1969 during Hurricane Camille (Bea et al. 1983).

This event triggered a series of analytical efforts (e.g. Wright and Dunham 1972; Scott and Zuckerman 1970; and Henkel 1970) to assess seafloor instability from waves. One of the first studies (Henkel 1970) considered a slip circle total stress analysis and showed that given the soil and water depth conditions in the South Pass region, the wave conditions during Camille could cause instability to significant depths.

In addition to the analytical work field measurements were made (e.g. Bennett 1977 and Bennett and Faris 1979) in GoM sediments to try and assess both the state of consolidation and excess pore water pressures from the wave loadings. Other field measurements were also made (Cross et al. 1979) in other parts of the world to assess the pore water pressure response for more cohesionless sediments. In addition to these field measurements additional analytical models were proposed to better understand the overall seabed response. For example, Liu (1973) considered a rigid seabed with incompressible pore fluid and hydraulic isotropy and derived the following expression for pore pressure decay within a finite seabed:

$$p = p_o \cosh \lambda (d_s - z)/(\cosh \lambda d_s) \quad [12]$$

Where $p_o$ is the pressure at the seabed, $\lambda$ is the wave number $(2\pi/L)$ where $L$ is the wavelength, $d_s$ is the thickness of the soil deposit and $z$ is positive downward into the seabed.

This equation was modified by Sleath (1970) to consider differences in the horizontal versus vertical permeability.

In 1978 a significant advancement occurred when Yamamoto (1978) and Madsen (1978) developed a coupled pore fluid-seabed approach to determine the effective normal and shear stresses. Their solutions considered the compressibility and degree of saturation of the pore fluid, and the elastic stiffness of the soil skeleton as well as hydraulic anisotropy. Their solutions allowed the determination of the phase lag between the bottom pressure and the various stress responses within the seabed.

Significant physical model testing has been performed to verify these analytical models and identify the most important variables affecting the stability of the seafloor. Some of these important tests are discussed below.

### *Model Tests-Clay Soils*

After the observed slope failure from Hurricane Camille, Doyle (1973) performed a series of small wave tank tests to observe the wave-induced instability. Tests were performed with a linearly increasing shear strength profile of underconsolidated clay and a profile with an upper crust to simulate upper crusts observed in the field resulting from the downslope movement of intact blocks. Tests to observe the seabed response were performed in water depths of 0.62 m. with a soil clay thickness 1.07 m. Combinations of wave periods and heights of 0.86 s/7.9 cm and 1.11 s/5.0 cm were investigated.

Failure depths ranged from 0.25 m to 0.99 m. For the underconsolidated increasing soil profile the failure depth and horizontal shear stress below the mudline was more accurately predicted with elastic theory. Henkel's slip circle analyses, however, reasonably predicted the depth of failure and the bottom pressure required to cause failure for the soil profile with an upper crust, although the failure surface was not entirely circular.

Doyle (1973) discusses in detail additional observations from the tests, including:

1. With repeated loaded the depth of failure reached an equilibrium state.
2. Remolding of the soil within the failed zone was gradual which led to the greater displacements within the failed zone. However, the depth of failure was reached in a relatively short period of time.
3. The vertical soil movements decayed much more rapidly than the horizontal movements.
4. Test performed with a mild slope resulted in downslope movement of the soil.

Although these tests were quite small and did not fully match similitude conditions for the 21.3 m plus waves (70 ft) generated by Hurricane Camille, they did provide physical evidence that bottom pressures generated by ocean waves could produce seabed instabilities. Despite their limited dimensions the tests did provide key insights regarding the basic failure mechanisms of these soft deltaic sediments.

### *Model Tests -Sandy Soils*

Several laboratory tests have been performed to determine the pore pressure response in sandy soils. The progressive build-up of pore pressures in these tests was not observed due to the limited wave heights and rapid pore pressure dissipation rates.

Clukey (1983) summarized (Table 2) previous model tests performed to assess the steady state pore pressure response in the sandy soils. These studies can be divided into 'small' and 'large' scale tests. The small-scale tests are characterized by relatively small wave heights

(<0.06 m) and/or wave periods less than 4 s. The 'large' scale tests had wave heights up to 2.4 m and wave periods up to 8.84 s.

**Table 2. Summary of selected previous wave tank tests in sand**

| Investigator | Hydrodynamic Parameters | | | | Soil Parameters | | | | | |
|---|---|---|---|---|---|---|---|---|---|---|
| | Water Depth (m) | Wave Ht. (m) | Wave Period (s) | Wave Length (m) | Soil Type | Depth (m) | $D_{50}$ (mm) | $kx10^{-1}$ (mm/s) | Void Ratio | $D_r$ (%) |
| Small-scale tests | | | | | | | | | | |
| Sleath (1970)[1] | 0.11-0.36 | 0.01-0.64 | 0.51-3.14 | 0.38-5.78 | Coarse sand | 0.33 | 1.13 | $k_z$=88.5 $k_x$=126 | 0.67 | - |
| | 0.15-0.30 | 0.01-0.04 | 0.59-6.92 | 0.51-11.48 | Fine sand | 0.33 | 0.46 | $k_z$=14.5 $k_x$=12.6 | 0.79 | - |
| Tsui and Helfrich (1983)[2] | 0.49 | 0.02-0.06 | 1.00-4.00 | 1.89-9.14 | Med. Sand-loose | 0.33 | 0.95 | 1.3-2.0 | 0.96 | 30 |
| | 0.49 | 0.02-0.06 | 1.00-4.00 | 1.89-9.14 | Med-sand-dense | 0.33 | 0.95 | 1.3-2.0 | 0.68 | 96 |
| Yamamoto et al. (1978)[1] | 0.90 | - | 1.00-2.60 | - | Coarse sand | 0.50 | 1.20 | - | - | - |
| | 0.90 | - | 1.00-2.60 | - | Fine sand | 0.50 | 0.20 | - | 0.54 | - |
| Large scale tests | | | | | | | | | | |
| McDougall et al. (1981)[1] | 2.44 | 0.21-1.34 | 1.77-8.84 | - | Fine sand | 0.91 | 0.20 | 0.70 | 0.70 | - |
| Lindenberg et al. (1982)[3] | 5.00 | 2.40 | 5.00 | | Fine sand | 2.50 | 0.15 | - | - | 70 |

[1] Progressive waves; [2] Stokes 2nd order waves; [3] Standing waves

## *Small Scale Tests*

As an example of the 'small' scale experiments, the results from Sleath (1970) are shown on Fig. 3. The y-axis on this plot are the measured pressure , $P$ , values normalized by the pressure at the top of the bed, $P_o$, determined from linear wave theory while the x-axis are the Sleath predictions considering hydraulic anisotropy $(k_x/k_z = 1.4)$. In this figure, $\lambda$ is the wave number $(2\pi/L)$, $d$ is the depth of the bed and $z$ is the coordinate measured upwards from the top of the bed. The value of 1 on the x-axis corresponds to the top of the deposit while 0 corresponds to the bottom of the deposit. Values of $P/P_0$ greater than 1 at the top of the deposit indicate higher measured values than predicted from linear wave theory through the water column.

At the top of the deposit the measured pore pressure attenuates at a faster rate than predicted by theory. As will be discussed later the more rapid the pore pressures attenuate, the greater the increase in the effective stresses within the bed. Below x-values of about 0.8 the agreement between theory and measurements appears relatively good.

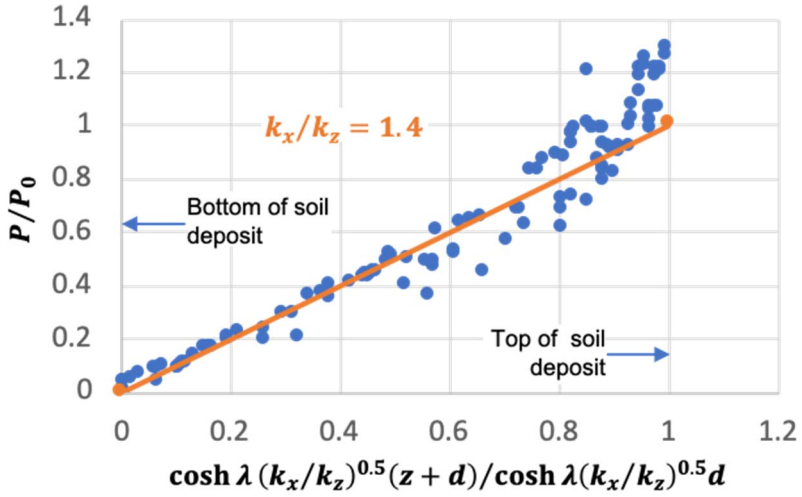


**Fig. 3. Pore pressure attenuation through bed of coarse sand with hydraulic anisotropy of 1.4. (modified from Sleath 1970)**

Clukey (1983) also performed tests and compared measured values to Liu's (1973) and Yamamoto's (1978) solutions (Fig. 4).

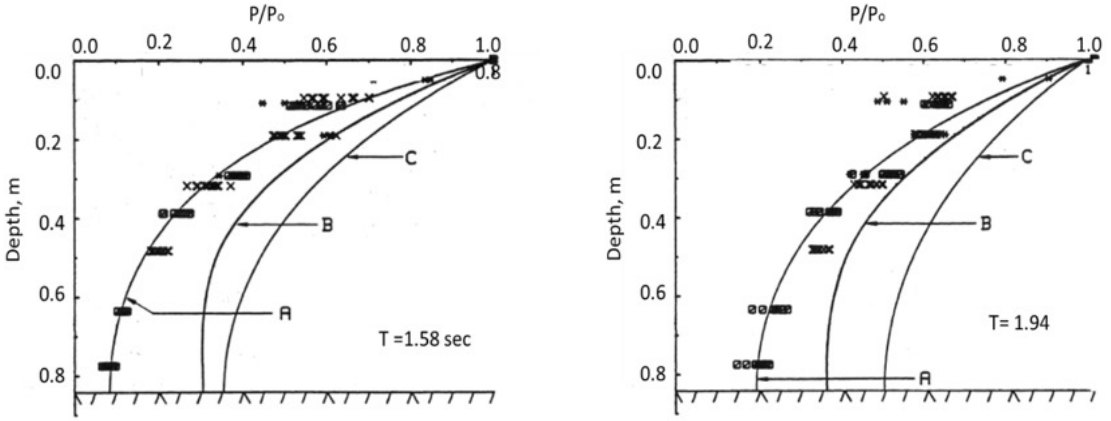


**Fig. 4. Pore pressure attenuation at two wave periods (from Clukey 1983) showing best fit to measured data (A) versus Yamamoto (1978) theory (B) and Liu (1973) theory (C).**

The agreement was better versus the Yamamoto theory although, like the Sleath results, the pore pressure attenuation was greater than predicted by theory.

### *Large Wave Tank Tests*

A series of tests were performed in the large 122-m (400-ft) long wave tank facility at Oregon State University with wave periods ranging from 1.77 to 8.84 s. (McDougall et al. 1981). These test results were also compared to the Yamamoto solution with different assumptions concerning the slip condition at the base of the deposit. In these tests, a 0.30-m (1-ft) gravel layer was placed on top of a fine sand.

The results show relatively good agreement with the full slip (free) condition and an overprediction of the pore pressures for the no slip condition (fixed condition). Once again there is an overprediction of the pore pressures near the top of the soil deposit.

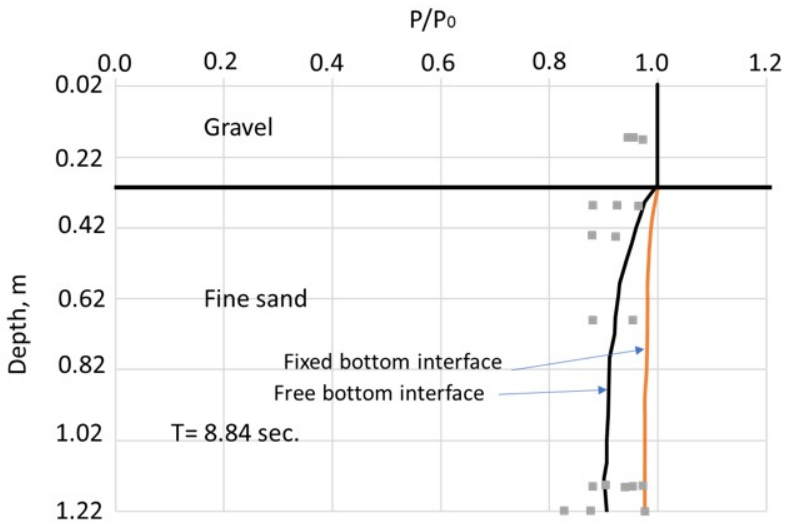


**Fig. 5. Large wave tank experiments at Oregon State- pore pressure attenuation comparisons with Yamamoto (1978) solution for fixed and free interface conditions at bottom of sand deposit. (modified from McDougall et al. 1981)**

The impact of bottom boundary conditions proposed by McDougall is interesting. Without interface tests on the sand and the bottom material in the wave tank it is not possible to determine the interface friction. However, it does not appear that the interface friction would be zero and the discrepancies between the measured values and theory at full friction (fixed) may be more realistic.

Overall, these three sets of tests suggest that the pore pressures may be impacted by: 1) hydraulic anisotropy, 2) saturation levels in the sand, or 3) bottom boundary conditions. In addition, Silvestri et al. (1985) have shown, using the Yamamoto/ Madsen models, very large reductions in pore pressures occur as the ratio of horizontal to vertical soil stiffness $(E_h/E_v)$ decreases. Reductions in the pore pressure response of over 50% occurred when the stiffness ratio decreased to 0.5. These stiffness considerations in addition to the general non-linearity of the soil are also likely contributors to the observed differences.

## *Effective Stresses and Sediment Transport*

The effective stresses and their corresponding shear stresses are perhaps of more interest than just the wave-induced steady state pore pressures. Theoretically the effective stresses may be determined with either an uncoupled or coupled approach. The uncoupled approach independently determines the total stresses and then subtracts the steady states pore pressures. The coupled approach developed by Yamamoto (1978) and Madsen (1978) is discussed above.

Experimental results determined by Clukey (1983) provide comparisons with the coupled theory. In these tests, the permeability of the sand was determined by the Kozeny-Carman relationship (Loudon 1952) while the sand density and degree of saturation were based on density-cup measurements in the wave tank. The elastic shear modulus was determined from simple shear tests and the bulk modulus of the water was estimated from the degree of saturation and seismic p-wave measurements made in the wave tank.

Measured effective stresses were determined by measurements of both the total vertical and horizontal stresses and pore pressures and the spatial relationships between the sensors. Comparisons between the measured and predicted effective stresses are shown on Fig. 6 - for a wave period of 1.58 s (wavelength of 3.11 m). Other tests were also performed with wave periods of 1.32, 1.94 and 2.49 s, respectively. The measurements were made in a sediment

bay 4.47-m long and 0.84-m deep located approximately in the middle of a 16.8-m long wave tank (Clukey 1983).

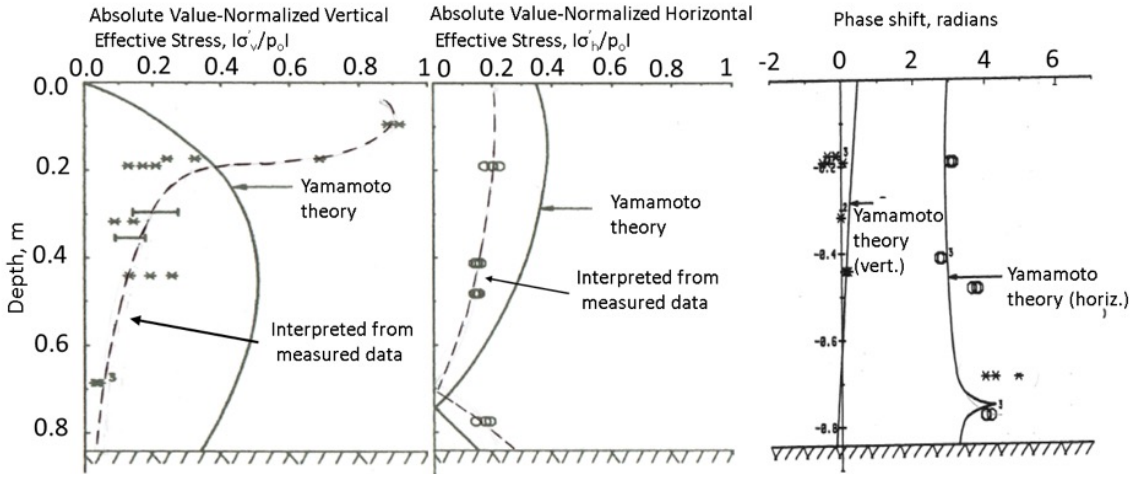


**Fig. 6. Effective stresses and phase shift (from Clukey 1983) for wave period (*T*) of 1.58 s**

As shown on Fig. 6, the magnitude of the normalized measured vertical effective stresses is significantly greater than values predicted from theory in the uppermost 0.10 m to 0.20 m; similar results were observed for the tests performed with a wave period of 1.94 s. For the other wave periods instrument failures prevented obtaining data at shallow depths. Below about 0.20 m the normalized effective stresses are significantly below the Yamamoto predictions. The phase relationships for the normalized vertical effective stress are in good agreement with predictions to about 0.50 m depth and suggest negligible phase shift with the bottom pressure. At about 0.70 m. depth this phase shift is about 4 radians. Similar phase shifts at this depth were also observed for the tests performed with wave periods of 1.94 and 2.49 s. This phase shift may be related to the proximity of the bottom boundary.

The normalized measured horizontal effective stresses appear to follow a similar but lower trend compared to the predictions. The phase shift for the normalized horizontal effective stresses are generally in agreement with the predictions. Similar tends were observed for the other wave periods.

Using the results from the largest sized waves for the tests with a wave period of 1.58 s to determine the effective stress in both the vertical and horizontal directions, the stability of the bed during the wave action can be evaluated. This stability assessment was made to assess the approximately 2 cm high sand ripples (Fig. 7) observed at the end of testing.

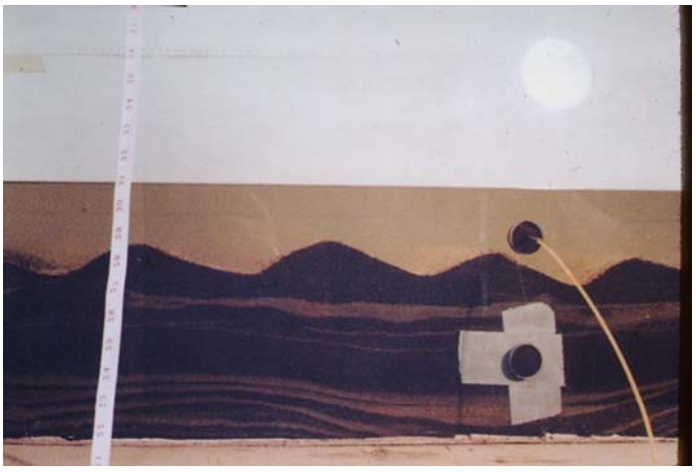

**Fig. 7. Approximately 2 cm high sand ripples observed at end of sand tests (Clukey 1983)**

One possible explanation for these features is that they were formed from traditional sediment transport mechanisms from a fluid-induced interface bottom shear stress between the water column and sand bed.

Alternatively, these features could occur from a bed failure resulting from changes in effective stresses. Yamamoto (1978) considered this mechanism, for a 24 m wave height on a sand seabed in 70 m of water. He reported the potential for failure as defined by the development of negative principal stresses, to a depth of about 1.5 to 2 m. This type of failure is not difficult to reconcile given the large wave height, relatively shallow water and long wavelength ($L = 324$ m) which would limit the attenuation of the wave energy to the seafloor.

However, the effective stress results shown on Fig. 6 were for considerably more modest waves (~0.25 m) which represent far less extreme conditions than those considered by Yamamoto. The Mohr-Coulomb stress circles based on the above results are shown on Fig. 8 for depths below the top of bed of 2 cm, 5 cm and 20 cm. Also shown on Fig. 8, for reference, is the effective stress friction angle for 40°. Figure 8(a) and (b) both show that as the trough of the wave passes the vertical effective stresses transition from the major to minor principal stress. However, as the overburden increases to 20 cm the vertical stress remains the major principal stress as the wave trough passes.

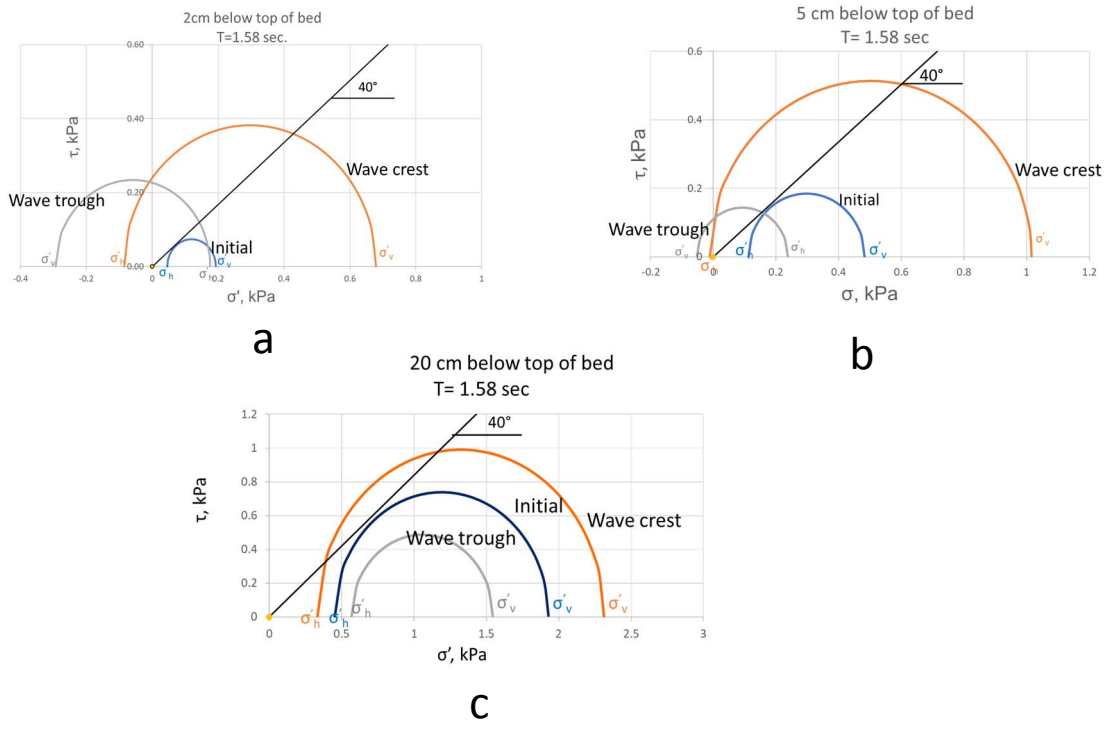


**Fig. 8. Mohr-Coulomb stress circle for 2 cm, 5 cm and 20 cm depth below top of bed**

At a depth of 2 cm significant negative (tensile) stresses are observed when both the wave crest and trough pass. Therefore, for significant portions of the time for each wave cycle the soil is in a 'failed' state (per Yamamoto's definition) and susceptible to movement. At a depth of 5 cm the soil is only in the 'failed' state for a short period as the trough passes and the vertical stresses becomes negative. Therefore, at this depth much less soil movement would be expected. At the 20 cm depth no negative stresses were observed, and the sand bed appears to be stable.

The results. suggest that the stress analysis is consistent with the observed sand ripple depth of about 2 cm, further indicating that changing effective stresses in a sandy seabed may cause instability and sediment transport. Transport initiated with this more soil-based mechanism coupled with the interface shear stresses would result in enhanced erosion.

### *Progressive Wave Liquefaction - Centrifuge Tests*

Wave induced liquefaction has been an offshore geotechnical topic of interest for over forty years. Bjerrum (1973) and Lee and Focht (1975) examined wave-induced liquefaction of the Ekofisk tank in the North Sea. On a much smaller scale, Dalrymple (1979) cited the impact of breaking waves and liquefaction on mega-ripples as the likely cause of internal deformation and cross bedding. Dalrymple further notes that breaking waves can impart fifteen to eighteen times more force than the hydrostatic force from a non-breaking wave. Zeevaert (1958) cited the failure of rubble mounded jetties overlying fine sand as the result of spontaneous liquefaction when the trough of the wave passes the toe of the jetty.

To consider wave-induced liquefaction Sassa and Sekigushi (1999) performed wave tank centrifuge tests on a fine sand. In these tests, time scaling laws for both wave propagation and consolidation drainage were properly scaled by using higher wave frequencies and a pore fluid with a higher viscosity than water. The scaling relationship for frequency and viscosity between the model and prototype in these tests were the following:

$$\omega_m = N\omega_p \qquad [13]$$

$$\mu_m = N\mu_p \qquad [14]$$

Where $\omega$ is the angular wave frequency, $\mu$ is the dynamic viscosity of the pore fluid and $N$ is the centrifuge acceleration factor (50). The tests were performed with a prototype water depth of 4.5 m, wave period of 4.5 s and wave height of 1.56 m. The test bed had a prototype thickness of 5 m. Initial tests started with a relative density $(D_r)$ of about 40% and liquefied throughout the deposit (Fig. 9a). As shown, the pore pressures increased continually with increased cycles and reached the overburden levels at all depths at 46 cycles. The critical stress ratio $(\tau_h/\sigma_{vo})$ to cause liquefaction was about 0.14.

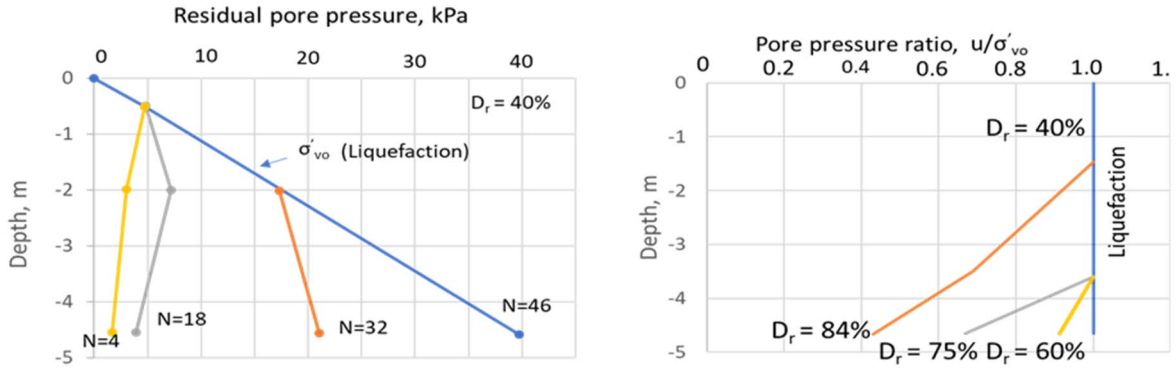


(a) (b)

**Fig. 9. Liquefaction test results (from Sassa and Sekigushi 1999) showing (a) pore pressure response for sand with relative density $(D_r)$ of about 40% and (b) after densification**

Figure 9b shows the pore pressure as the relative density of the sand changed between successive test runs. The relative density of the sand changed between tests due to consolidation between tests. After the initial liquefaction the relative density increased to 60%

and most of the deposit again liquefied although there was a slight decrease in the maximum pore pressure at 4.75 m. Once the relative density increased to 75% this reduction in pore pressure at 4.75 m was more substantial. At a relative density of 84%, both the pore water pressures at 3.5 m and 4.75 m continued to decrease. However, the pore pressure at about 1.5 m continued to reach liquefaction levels at all relative densities. It should be noted that the relative densities described by Sassa and Sekigushi (1999) represent averages of relative densities which could vary with depth in the deposit.

This densification of the seabed has also been documented through analytical studies and field studies. Degroot and Meijers (1992) showed that the densification that occurs during a storm event in build-up to the larger sized waves that cause liquefaction should be sufficient to prevent liquefaction. In a field experiment Clukey et al. (1989) measured the increase in density with a small penetrometer for a freshly deposited sand in about 9 m of water and observed an increase in relative density from about 57% to 90% over a 5-month period.

### *Wave Induced Liquefaction-Silt Tests*

Clukey et al. (1983) were interested in understanding wave-induced liquefaction's contribution to the large amounts of sediment transport of the silty soils from the Yukon delta. They performed tests on silty soils in the same wave tank facility used for the sand tests discussed above. These tests were performed in 0.53-m water depth with wave heights ranging from 0.10 m to 0.30 m and wave periods ranging from 1.76 to 2.02 s. The results of the pore pressure response for the 0.10 and 0.30 m wave heights are shown on Fig. 10. These pore pressure results (Fig. 10) were recorded at 0.23 and 0.28-m depths respectively, below the top of a 0.84-m deep silt deposit.

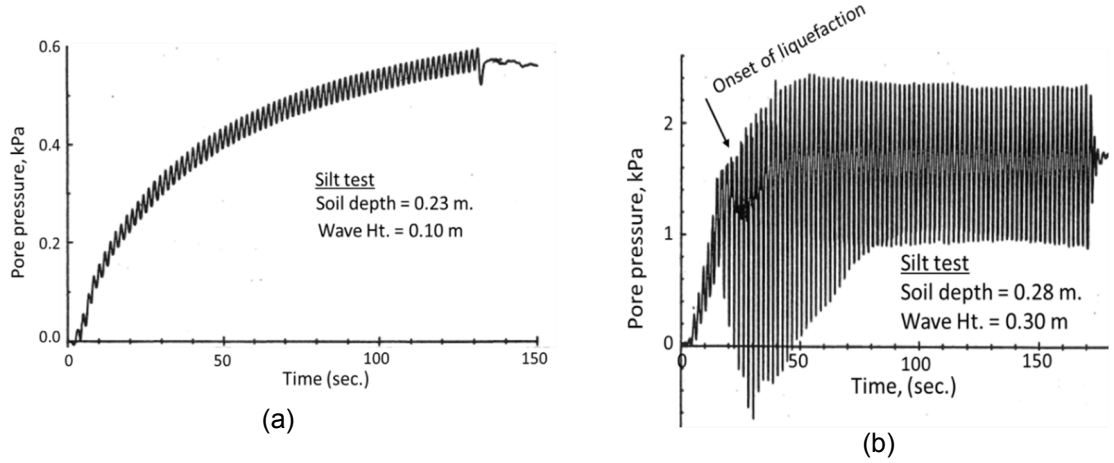


**Fig. 10. Pore pressure results from silt tests (from Clukey et al. 1985).**

Figure 10(a) shows the progressive buildup to about 0.58 kPa without reaching a liquefied state. Figure 10(b) shows the progressive buildup to a mean value of about 1.7 kPa where the bed was observed to fail. The measured pore pressure ratio $(u/\sigma'_{vo})$ at this point was 0.70. Overall high pore pressures ratios occurred 0.10 m. to 0.62 m. below the mudline and ranged from 0.62 to 1.08. The average pore pressure ratio in this depth range was 0.75.

Additional evidence of high pore pressures was based on observations of numerous mud volcanoes on the surface of the bed following the test (Fig. 11).

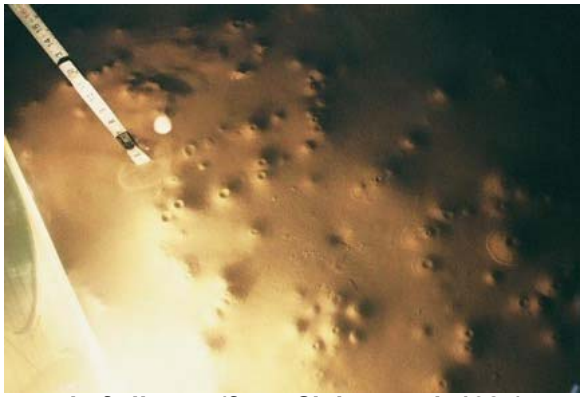

**Fig. 11. Mud volcanoes at end of silt test (from Clukey et al. 1985).**

Clukey (1983) also noted that at the beginning of the tests a 5/8" rod was easily pushed to the bottom of the deposit with hand pressure. At the end of the test, however, much greater pressure (about 30 kN) was required to push the same rod through a zone starting several centimeters below the mudline and extending to slightly above the midpoint of the deposit. This observation again suggested densification near the top of the deposit.

Based on these results Clukey (1983) proposed a model whereby freshly deposited silt in the Yukon delta would be highly susceptible to wave-induced liquefaction, particularly in years of deposition with large storm events. However, in years with more moderate events the silt would likely densify and be less prone to liquefaction and transport in future years.

## MUDSLIDE, DEBRIS FLOW AND TURBIDITY CURRENT IMPACT ON PIPELINES

Offshore pipelines and flowlines are often sited in regions with relatively high seafloor slopes and potential submarine slumping (e.g. Berger et al. 2006). Once a slope fails it can potentially stabilize with limited displacements as the slope angle decreases or it could also move downslope significant distances with high velocities as the strength of the soil is reduced along the sliding surface. This movement can also be enhanced by hydroplaning (Narbitz et al. 2003) as the slide moves further downslope. Slide movements on the order of hundreds of meters to kilometers with limited water entrainment during the sliding process are often referred to as debris flows. If additional water is entrained during the sliding process, the slide material may be supported by the turbid nature of the flow. This type of mass turbidity flow can travel as much as tens to, in extreme cases, thousands of kilometers at high speeds.

Pipelines in the path of these mass transport flows can be at risk from potentially high impact forces. For many years the approach taken to mitigate this risk was: 1) re-route the pipeline to avoid the hazard or 2) orient the axis of the pipe in the direction of the flow to minimize bending loads. In many cases, particularly for very large flow events, the first approach is still prudent since it is often not reasonable to expect that pipelines can perform as designed under such adverse conditions.

It should also be noted that in the early years of the offshore industry models did not exist to predict run-out distance and velocities of mass flows. With the advances made in large deformation numerical methods and Computational Fluid Dynamics (CFD) these predictions can now be made. A significant challenge though for assessing the pipeline response is the determination of the forces imparted by a mass flow on the pipeline.

The direct impact forces of a flow on a pipeline were investigated experimentally by Zakeri (2008) and by Zakeri et al. (2008) with a series of flume experiments. By varying the density of the flow material, the slope of the bottom and the constant head driving the flow they were able to achieve a wide range of non-Newtonian Reynolds numbers, defined as:

$$Re_{non-Newtonian} = \frac{\rho v_n^2}{\tau} \quad [15]$$

Where $\rho$ is the density of the flowing mass, $v_n$ is the flow velocity perpendicular to the pipe and $\tau$ is the mobilized shear stress at the pipe, which will vary with: 1) the rate of flow, 2) clay concentration, and 3) the changing water content of the flow. The Reynolds numbers investigated covered a range of different flows encountered in the field and demonstrated how small experiments can properly simulate field conditions with appropriate scaling.

Zakeri (2008) characterized the normal force on the pipe as:

$$F_n = C_d \left(\frac{1}{2}\rho v_n^2\right) D \quad [16]$$

Where $C_d$ is the drag coefficient and $D$ is the pipe diameter. The drag coefficient varies with the Reynolds number defined above.

The experimental set up for these tests is shown on Fig. 12. Tests were performed with an elevated pipe and a pipe resting on the floor of the flume. The flow velocities were measured with high speed cameras while both the vertical and horizontal forces on the pipeline were measured with load cells. A sonar device was used to monitor the height of the flow. The results for the elevated pipe, where the flow engulfed the pipe, are shown on Fig. 13.

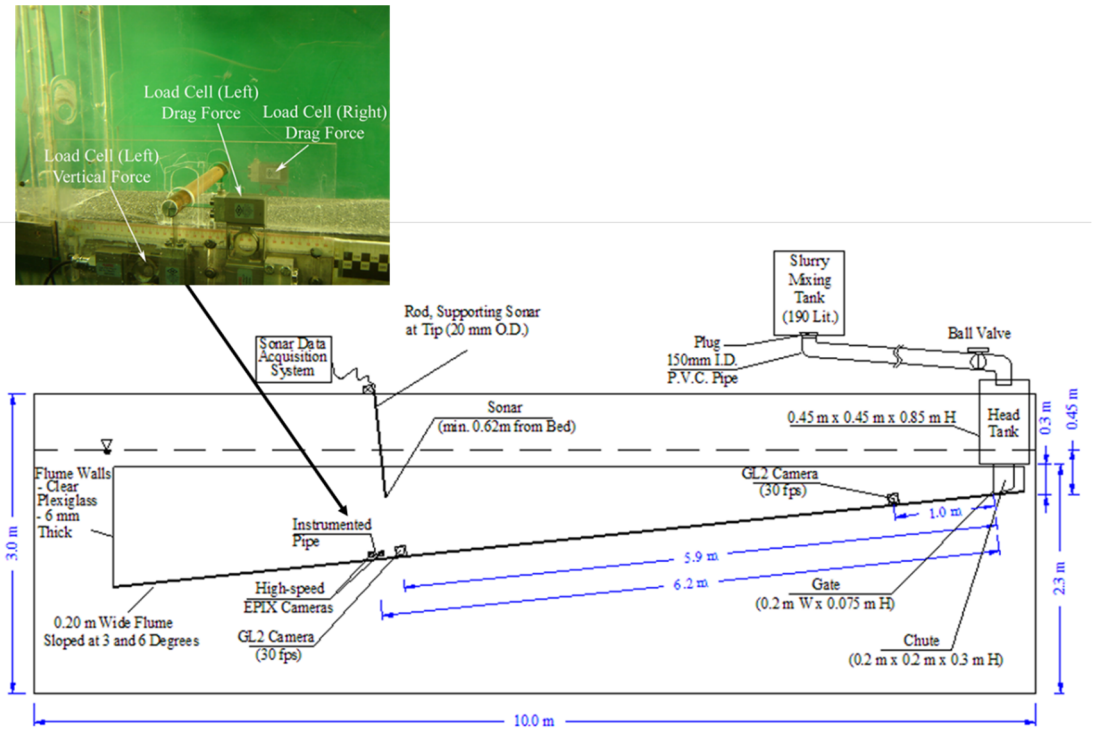


**Fig. 12. Experimental set-up for tests to determine debris flow impact on pipelines (from Zakeri 2008)**

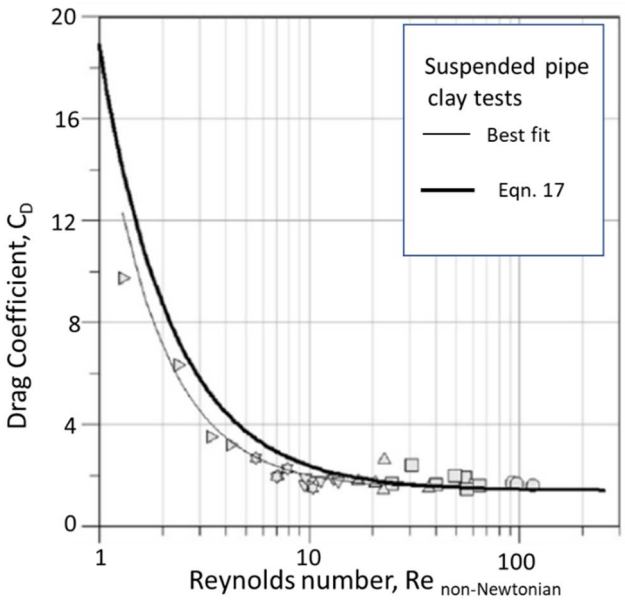


**Fig. 13. Experimental results from debris-flow pipe impact study (from Zakeri 2009)**

Based on this data the following relationship between the drag coefficient and the Reynolds number was developed:

$$C_D = 1.6 + \frac{12.8}{Re_{non-Newtonian}^{1.45}} \quad [17]$$

Zakeri (2009) coupled these results with CFD analyses and found very good agreement between the two approaches (<10% difference) for Reynolds numbers greater than 10. For Reynolds number less than 10, CFD results overpredicted the $C_d$ by about 15% to 25% - still very good agreement. The agreement between the experimental and CFD results allowed Zakeri to confidently extend the CFD results to different attack angles on the pipeline. The drag forces in the experiments with pipes resting on the floor were found to be about 20 to 30% less than the experiments with the suspended pipes.

Randolph and White (2012) used the Zakeri data and separated the force imparted on the pipe into a velocity dependent drag term and a bearing term as shown below:

$$F_n = C_d \left(\frac{1}{2}\rho v_n^2\right) D + N_p S_{u,nom} D \quad [18]$$

Where $N_p$ is a bearing capacity factor and $S_{u,nom}$ is a velocity dependent shear strength. In their formulation the drag coefficient does not depend on the Reynolds number and is equal to 0.4 while the bearing capacity factor, $N_p$, is 13.

Randolph and White (2012) also provide a method for estimating the friction force along the axis of the pipe for flows approaching at oblique angles to the pipe as well as procedures for determining the interactions between the normal and axial forces.

Zakeri (2012) also investigated the impact of intact glide blocks on a pipeline. In this case centrifuge model tests were performed. A total of eleven test were performed at shear strengths ranging from 4.2 kPa to 80.0 kPa, impact velocities from 0.2 to 1.0 m/s and a centrifuge acceleration of $30g$. Based on the experimental results Zakeri also defined a bearing capacity factor that is rate dependent where the strain rate $\gamma'$ ($s^{-1}$ units) is defined as the upstream velocity, $V$, divided by the pipe diameter, $D$. Although the strain rate in the centrifuge is $N$ (30) times greater than the prototype the strain rates investigated in the tests

provided a range of values applicable to field conditions. The bearing capacity factor $N_p$ and the normal force on the pipeline are then defined as:

$$N_p = 7.5\gamma'^{0.112} \quad [19]$$

$$F_n = N_p S_u D \quad [20]$$

## SUCTION CAISSON AND BUCKET FOUNDATIONS

### *Overview*

Beginning in the early 1990s, the offshore industry expanded into deeper water and structures changed from fixed steel piled jackets to various types of floating facilities. Suction caissons then became a viable foundation alternative. Although, like piles the foundation soil resistance for suction caissons is comprised of side friction and end bearing, there are several significant differences (Clukey, et al. 2013), e.g.:

- Due to different installation methods and geometry the magnitude and set up times for side friction are different.
- The governing design loads are uplift versus compression for piles used on steel piles jackets.
- The (reverse) end bearing provides a much greater proportion of the total soil resistance.
- The magnitude and in some cases duration (e.g. loop currents in the GoM) of loads are different.
- Cyclic loading effects have greater potential for more damaging two-way loading.
- The foundation system is generally less redundant than piled systems for steel piled jackets.

Physical model testing has played a significant part in addressing many of these issues and eventually developing robust approaches now used in design (API RP 2SK, 2005 and ISO 19901-4, 2011).

The first applications were in the North Sea for the Snorre and Heidrun Tension Leg Platform (TLP) projects. Model tests were performed to verify these designs. These tests as well as others to extend the technology to deeper water in other parts of the world are described below. In addition, tests to address wind tower designs in sand are also presented.

### *Suction Caisson Model Tests in Clays*

#### Capacity Considerations

Model tests (Fig. 14) were performed (Andersen et al. 1992; 1993) on a 4-cell cluster to verify the adequacy of the Snorre design. The tests (Fig. 14) were performed with about a 10:1 scaling relationship and considered loads inclined from vertical with cyclic components. The cluster consisted of 4 individual 0.91-m-diameter suction caissons attached together such that the width along each side was 1.83 m. The caisson cluster was embedded 0.90 m. The test results were satisfactorily analyzed with procedures developed by NGI and discussed by Andersen in his 2015 McClelland lecture (Andersen 2015).

Figure 14(a) shows the caisson cluster at the end of testing for an inclined uplift load while Fig. 14(b) shows the top surface of the clay after the caisson cluster had been extracted. Note the failure surface away from the caisson cluster footprint.


(a) (b)

**Fig. 14. Model tests to verify Snorre suction caisson design showing (a) caisson at failure (with permission from K.H. Andersen) and (b) soil plug after caisson removal.**

Morrison et al. (1994) performed centrifuge tests of the NGI Snorre tests to investigate the adequacy of centrifuge testing for addressing this problem. The tests were performed at a low $10g$-level. A comparison of the centrifuge results (for both kaolin and the Lysaker clay taken from the test site) are shown on Fig. 15. Overall these results provided confidence in using the centrifuge approach to investigate suction caissons in clay.

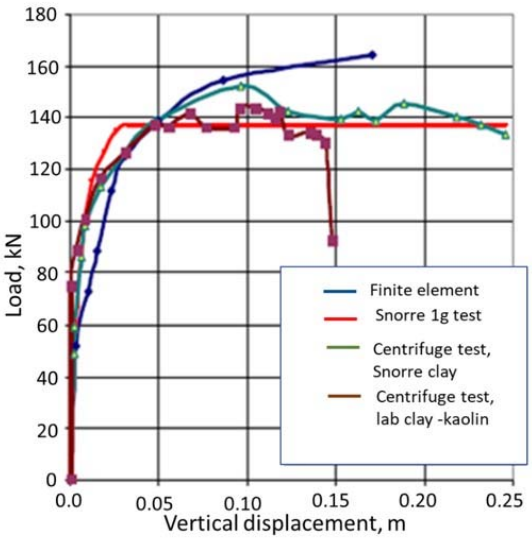


**Fig. 15. Comparison between Snorre, centrifuge tests, and finite element analyses (from Morrison et al. 1994)**

Exxon then initiated a model testing program to determine whether North Sea suction caisson technology could be transferred to the GoM. A comprehensive program was performed over several years, again aimed at a cluster type arrangement. Monotonic and cyclic tests were performed with uplift, slightly inclined and variable loading angles (Clukey and Morrison 1993 and Clukey et al. 1995). Some of the results from this testing program are shown on Fig. 16.

Figure 16(a) shows good agreement between finite element results (Clukey and Morrison 1993) and the centrifuge results while Fig. 16(b) show the interaction diagram between the static and cyclic loads (Clukey et al. 1995). Note that this interaction diagram could be used

as a design check for the methods proposed by Andersen (2015) where similar interaction diagrams are developed based on cyclic lab tests.

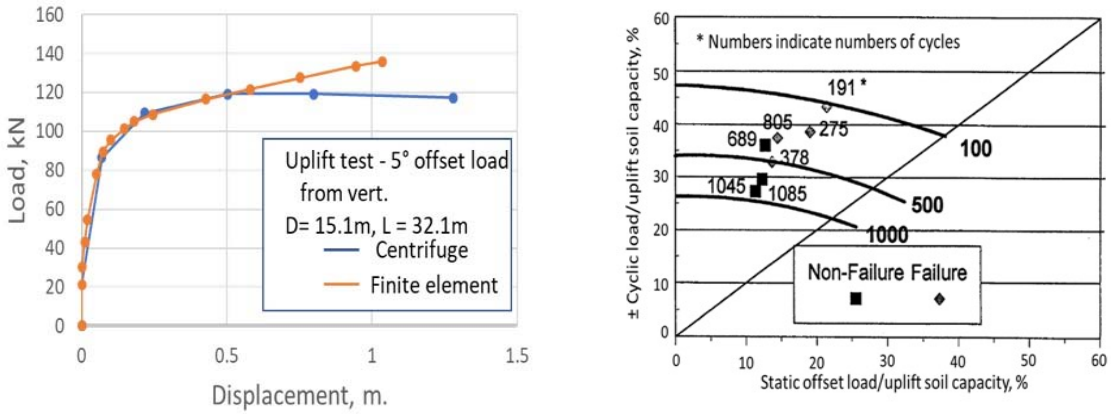


(a) (b)

**Fig. 16. Comparison between (a) centrifuge and finite element results and (b) interaction diagram for suction caissons in uplift (from Clukey et al. 1995).**

Suction caisson clusters, however, were never used in the GoM. Instead single cell caissons with length to diameter ($L/D$) ratios of 4 to 7 were used to anchor deepwater facilities once water depths exceeded about 1,200 m (Fig. 17). A considerable number of model tests were performed to investigate these foundations. However, for the deeper water applications the primary interest was for floating systems with catenary to taut moorings. These applications had considerably more horizontal loads versus the TLP applications.

Through a joint industry testing program by NGI the ability to resist the larger horizontal loads was found to be significantly enhanced by lowering the attachment point (Fig. 17) down the side of the caisson (Keaveny et al. 1994 and Andersen 2009). This testing program also showed that the cyclic capacity was less than the capacity for monotonic loading and there was some potential for a crack to form on the back side of the caisson. Lowering the attachment point such that the caisson rotated slightly backwards, however, mitigated the crack potential. The possibility of separation of soil from the trailing side of a suction caisson had been a concern in the industry for some time. Finite element analysis by Templeton (2002) had demonstrated this phenomenon and shown that separation was promoted by shallower water depths (i.e., low cavitation pressure) and by relatively high load attachment points.

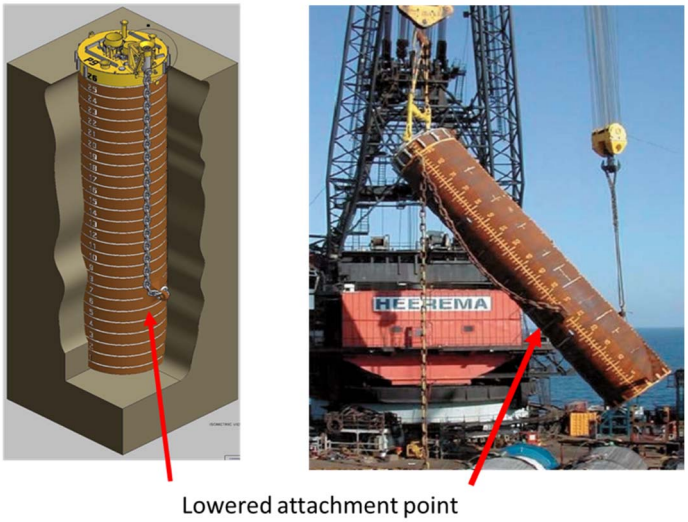


(a) (b)

**Fig. 17. Schematic (a) and typical (b) single cell suction caisson used to anchor deepwater facilities. Note: chain alongside is detached at top of caisson and attached to mooring line during final phase of installation.**

Despite the very useful information derived from the joint industry program, very little direct experimental data existed for the geometries and soil conditions relevant to the GoM. Additional centrifuge tests on 5.3 m diameter caissons were then performed at C-CORE (Fig. 18a) where the scaled prototype dimensions were very close to many of the planned suction prototype dimensions.

One of the goals of these tests was to determine potential differences in capacity, as discussed by Andersen and Jostad (2002), for caissons installed by direct pushing versus those installed by pushing followed by suction. A comparison of these test results is shown on Fig. 18b. After adjustments were made between the embedment length, load angle and the proportion of the caisson installed with suction, Clukey and Phillips (2002) estimated that the portion of the caisson installed with suction had about 25% less external skin than the caisson installed by pushing. This generally agreed with the analytical results by Andersen and Jostad (2002) who also showed a reduction in external skin friction for caissons installed with suction versus driven piles.

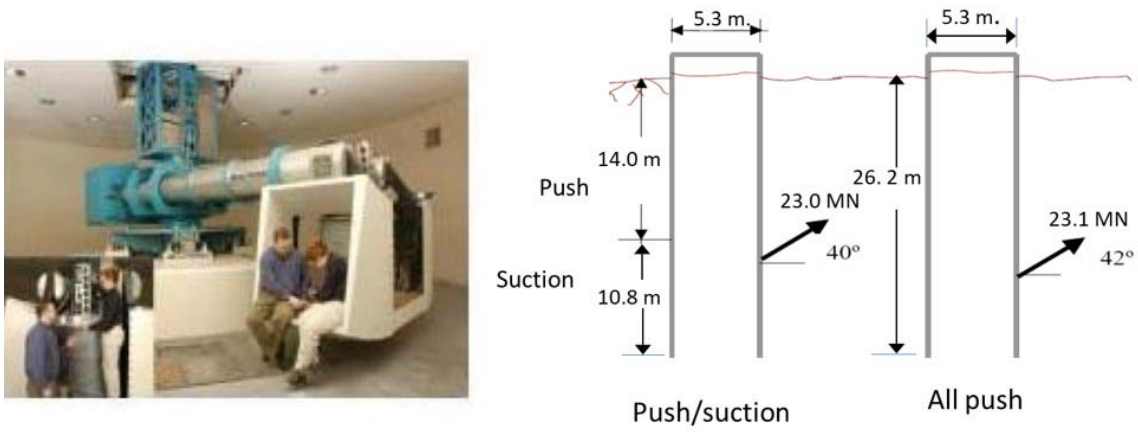


(a) (b)

**Fig. 18. C-CORE centrifuge facility (a) and results (b) of centrifuge test to verify suction caisson design (from Clukey and Phillips 2006).**

The measured capacities shown on Fig. 18b were 43% and 38% greater than predicted with the Design Method (DM) used to estimate the capacity for the test using both pushing plus suction and the test installed by pushing, respectively. This DM method used API recommendations for piles to estimate external side friction ($\alpha$ values) for the pushed portion of the caisson and the lower bound estimate of 0.65 (Andersen and Jostad 2002) for the portion installed with suction. A conservative (reverse) end bearing coefficient of 80% of API recommended values (Clukey and Morrison 1993) was also used. The greater measured capacities provided confidence in the design approach used at that time. These tests also showed no gapping on the backside of the caisson and further demonstrated the effectiveness of lowering the attachment point along the side of the caisson. These tests, however, did not separate the side resistance and reverse end bearing that comprise the soil resistance.

Subsequent tests by El Sherbiny (2005) and Jeanjean et al. (2006), however, did make these measurements by employing a double-walled caissons and instrumentation systems that isolated the side friction from the end bearing. The El Sherbiny tests were performed in normally consolidated kaolin clays on a 102 mm diameter suction caisson with an embedment length to diameter ratio of 8. Based on a comparison of tests installed directly with deadweight versus those installed with deadweight and about 50% suction the average external side friction $\alpha$ values were found to be 1.0 versus 0.91, respectively. With a linearly increasing shear strength profile and assuming an α value of 1.0 is applicable for the upper portion of the caisson installed deadweight, the 0.91 $\alpha$ value for the overall external side friction would be reduced to 0.87 for the portion installed with suction.

Jeanjean at al. (2006) performed centrifuge tests in kaolin soils with a double-walled caisson and prototype diameter of 1.88 m embedded to 11.25 m ($L/D = 6$). For three tests installed with 50% suction he determined an average external α value of 0.78. If the part of the caisson installed by pushing is assumed to have an α value of 1.0, then the average α value for the portion of the caisson installed with suction would be 0.71. However, for tests installed with only pushing the average α value was also 0.71. Therefore, the experimental data from these tests regarding the impact of suction on external skin friction appears to be mixed.

The average end bearing factor ($N_c$) at failure as determined by El Sherbiny (2005) based on two tests with a sealed top cap, was 12.5. This is similar to the 12.3 maximum bearing capacity factor (Fig. 19) determined by Jeanjean et al. (2006); however, at the displacement when failure occurred (1.3% of the caisson diameter), the bearing capacity factor was 9.0.

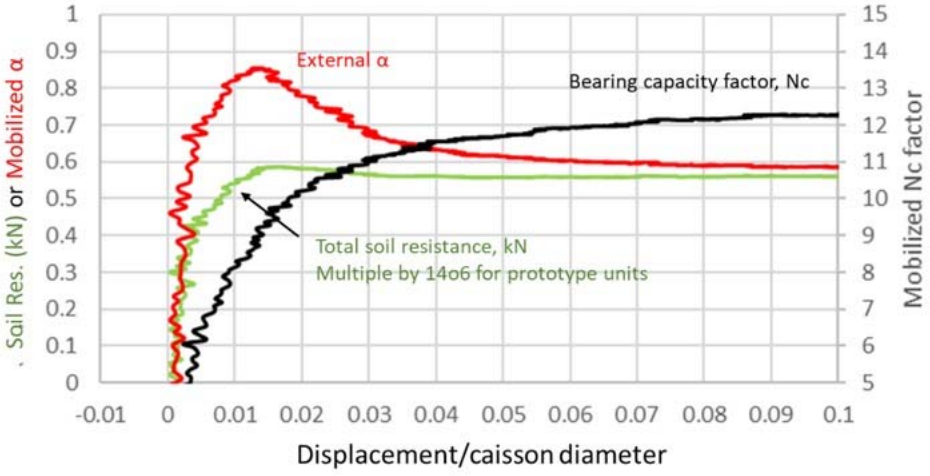


**Fig. 19. Experimental results showing independent measurements of skin friction and end bearing (modified from Jeanjean 2006)**

As shown in Fig. 19, significant softening occurs for the external side friction beyond 1% of the caisson diameter. This is compensated by the continual increase in reverse end bearing, resulting in only a modest decrease in the overall soil resistance.

House and Randolph (2001) also performed centrifuge tests in uplift on kaolin soils and deduced the bearing capacity factor by performing the tests without set-up and assuming the external side friction was based on the α value derived for installation. Based on these tests they derived a bearing capacity factor of 12. In the House and Randolph tests very little reduction of the external skin friction would be expected since the soil would be close to the remolded state.

Chen and Randolph (2005) also performed centrifuge tests on $L/D = 4$ caissons where they determined total (internal and external) side friction values from vented tests. They then used this average skin friction to assess the bearing capacity in sealed tests. The tests by Jeanjean (2006) and El Sherbiny (2005), however, both indicate significant differences between internal and external skin friction. The tests by Jeanjean indicate that the external skin friction is 26% greater than the average of the internal and external values. If the average skin friction values reported by Chen and Randolph are increased by 26% and combined with the results from Jeanjean et al. and El Sherbiny the following (Table 3) external skin friction $\alpha$ values and end bearing factors are derived.

**Table 3. Comparison of external side friction (S.F.) and reverse end bearing (REB)**

| | Jeanjean[1] | Chen and Randolph[1] | El Sherbiny[2] | Average | Std. Dev. |
|---|---|---|---|---|---|
| $L/D$ | 6 | 4 | 8 | | |
| # Tests for S.F. | 3 | 2 | 3 | | |
| External $\alpha$ | 0.78 | 0.88 | 0.91 | 0.85 | 0.06 |
| # Tests R.E.B. | 1 | 2 | 2 | | |
| $N_c$ ($S_u$ at tip) | 9/12.4[3] | 11.2 | 12.4 | 11.9 | 0.66 |
| $N_c$ ($S_u$ at $B/4$) | 8.6/11.5[3] | 10.5 | 12 | 11.3 | 0.76 |

[1] Centrifuge tests in normally consolidated kaolin
[2] 1-$g$ tests in normally consolidated kaolin
[3] Significant external skin friction softening, lower $N_C$ is at peak load
Note: All tests installed with 50% pushed and 50% suction and loaded axially in uplift

## Interaction Effects

As noted, suction caissons used for mooring applications will have inclined loads which result in an interaction between the vertical and horizontal components of capacity.

Aubeny et al. (2003) proposed an upper bound limit analysis approach to determine these interaction effects. This approach has been verified with experimental results by Clukey et al. (2003) and El Sherbiny (2005) as shown on Fig. 20. In both studies the load was applied at about 2/3 of down the embedment depth. The $L/D$ ratios were about 5 and 8 for the Clukey et al. and El Sherbiny studies, respectively. Both studies show that there is little interaction for loading angles, as measured from the horizontal, greater than 45°. The El Sherbiny results suggest no interaction for load angle as low as 30° while the Clukey et al. results suggest about a 10% reduction, versus full mobilization of the vertical capacity, at the 30° load angle.

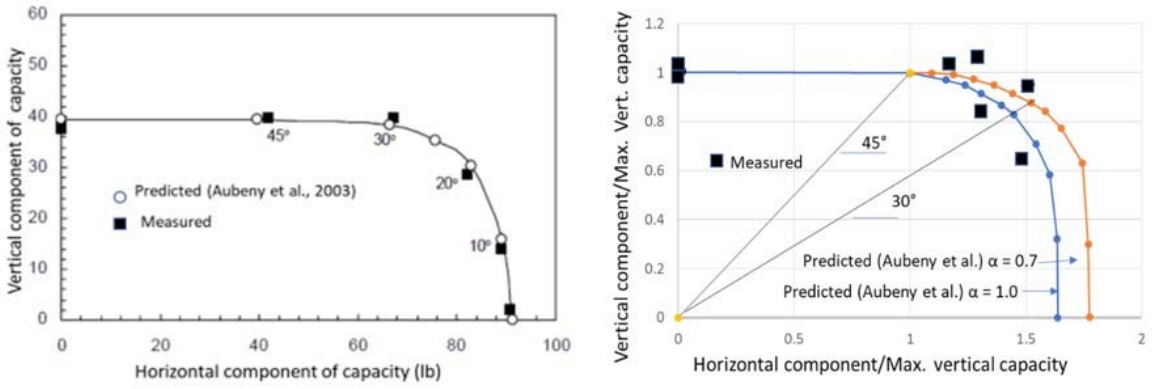


(a) (b)

**Fig. 20. Comparisons of analytical and experimental results from (a) El Sherbiny 2005 and (b) Clukey et al. 2003**

The actual loading angle for many practical cases can often be greater than the angles required to eliminate interaction effects because: 1) taut legged mooring systems will have high loading angles at the mudline, 2) the inverse catenary from the mudline to the pad eye will typically increase the angle from 4° to 8°, and 3) the caisson will be designed for a worst case forward tilt of about 5° which also adds to the design load angle. For cases where there is negligible interaction the soil resistance can be determined by simply dividing the soil resistance in uplift by the sine of the loading angle. For this case the external skin friction ($\alpha$) and reverse end bearing coefficients ($N_c$) shown on Table 3 could be used directly to assess the uplift resistance.

## Sustained Loads

Sustained loads are especially important in GoM where loop current loads can endure for several days (Vukovich at al. 1979) and can often be the governing design load. The potential impact of these loads on suction caisson holding capacity was investigated by Clukey et al. (2004) where the results of two independent centrifuge model studies (Clukey and Phillips 2002 and House 2002) and additional finite element analyses were combined.

The combined results are shown on Fig. 21 for suction caissons in kaolin. The centrifuge tests were performed by applying a load as a percentage of the short-term uplift capacity ($Q/Q_{ult}$), holding the load over time and observing the increase in vertical displacement. These tests were performed with embedment ($L/D$) ratios from about 3.9 to 4.8. The finite element results were performed with $L/D$ ratios of 5 and 7. Both the sets of tests show that although displacements continue to increase, they are maintained below 5% of the diameter for hold times approaching 100 days. The centrifuge test results generally suggest lower hold times than the GoM finite element analyses. This trend is expected due to the lower coefficients of consolidation ($c_v$) for GoM clay versus kaolin.

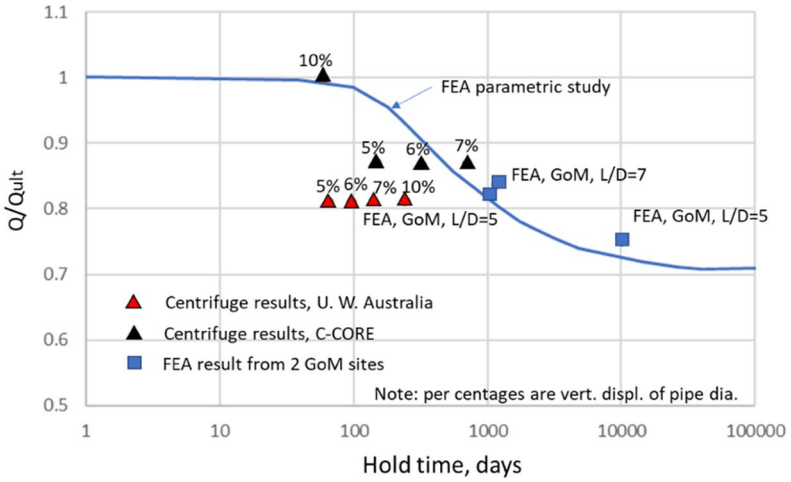


**Fig. 21. Test results to determine long-term holding capacity of suction caissons (modified from Clukey et al. 2004)**

The reduction in capacity with time is solely the result of a loss of 'suction effects' at the bottom of the caissons causing a corresponding reduction in reverse end bearing. It should be noted that for loop current designs the appropriate shear strength will be lower because of rate effects on the soil. However, the results on Fig. 21 show that for loop current load durations of 3 to 5 days the 'suction' required to mobilize reverse end bearing will not be degraded.

### *Suction Buckets in Sand for Wind Towers*

With the advent of offshore wind development emphasis has returned to offshore foundations in shallower water depths. Although offshore wind towers have been designed and installed in a variety of soil conditions the focus of this discussion will be on suction bucket (suction caisson) foundations in sandy soils.

Many of the initial designs were based on single monopiles or mono-buckets. These designs were for smaller (1-MW) wind towers and relied primarily on lateral resistance to resist loads and keep displacements within serviceability limits. As the offshore wind industry continued to evolve larger sized towers with much larger blade sizes (>50 m) have proven to be more cost effective. From a foundations perspective this has presented two options:

1. Continue using larger monopiles or buckets to resist the larger loads.
2. Convert to multi-leg structures better suited to resist increased overturning moments.

The first option, although feasible, can result in pile or caisson sizes that could present fabrication and installation challenges and increased costs.

For the second option the vertical resistance becomes more critical as the resisting moment increasingly results from the moment couple developed between multiple foundations. The foundation chould be designed such that uplift is prevented on the most windward foundation. In this case the foundation and structural weight would provide most of the uplift. Relying on just structural and foundation weight is a challenge though since offshore wind towers are substantially lighter than offshore jacket structures. Adding ballast will increase the uplift capacity but the operation will likely be performed offshore and as a result will be costly.

Suction caisson foundations in sand can potentially provide large amounts of soil resistance in uplift, although verifying this uplift has important technical challenges. First, due to the difficulties installing suction caissons to significant depths, resulting in relatively small $L/D$ ratios, the total skin friction will be relatively small. However, reverse ending bearing could be

very large because of the foundation diameter. The reverse end bearing will depend on the pore pressure response of the sand. Verifying the potential reverse end bearing to assure that rapid pore pressure dissipation will not reduce capacity is required.

To address this issue Nielsen et al. (2017) performed model tests on 0.5 m diameter ($L/D$=0.5 and 1.0) models and observed increased capacities by a factor ranging from 18 to 25 times the drained uplift capacity. Likewise, Byrne and Houlsby (2002) report a tenfold increase versus drained capacity for tests on 0.15 m diameter ($L/D$=0.33) models. However, both these studies note large displacements are required to mobilize these larger capacities.

An important consideration for assessing the reliability of the uplift capacity concerns the cyclic behavior. Houlsby et al. (2006) performed cyclic tests on a 1.5-m diameter ($L/D$=0.66) buckets in sand and observed a significant reduction in stiffness when tension loads were applied. They conclude that the results suggest that tension loads should not be applied due to unacceptable displacements and resultant serviceability considerations. They also note that at the largest cyclic loads (±100 kN) the net displacements were downward despite the large upward movement in each cycle.

Byrne and Houlsby (2002) also note the importance of load history and the sequencing of loads on the cyclic behavior. They use an innovative method to embed design events into pseudorandom events to produce time histories. Using this loading sequence for the 0.15-m ($L/D$= 0.33) caisson noted above they observed the following time history of vertical displacements (Fig. 22).

Although there is clearly a change in stiffness for the more extreme events, the maximum total displacements are relatively small (about 0.23%$D$ total). As noted by Houlsby et al. (2006) acceptable foundation rotations may be about 0.002 radians (0.12°). The structural rotation will, of course, depend on the foundation spacing. If 5 m diameter caissons were used and it was assumed that the rotational resistance was provided by the vertical resistance then, if the two caissons were separated by 20 m, the rotation would be only 0.0006 radians.

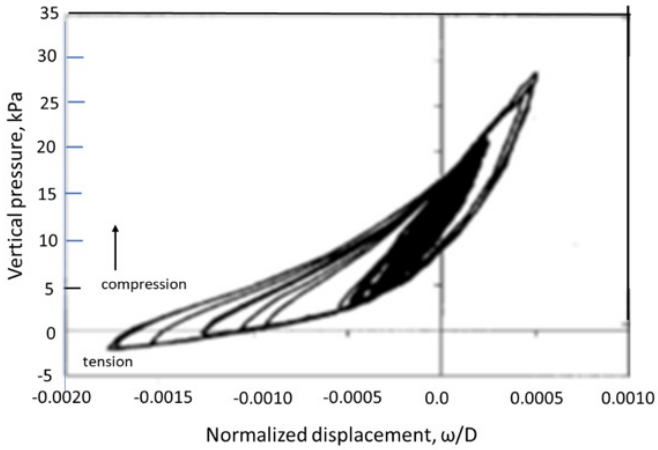


**Fig. 22. Cyclic loading test results (from Byrne and Houlsby 2002)**

Byrne and Houlsby (2002) correctly note the potential limitations of small-scale tests, and through dimensional analysis, for a light-weight structure where the mean load is small compared to the cyclic load, develop the following relationship for estimating foundation displacements.

$$\delta\sqrt{\frac{p_a}{V_m}} = f\left(\frac{V_p}{V_m}\right) \quad [21]$$

Where $\delta$ is the foundation displacement, $p_a$ is atmospheric pressure, $V_m$ is the mean cyclic load, and $V_p$ is the peak cyclic load. This expression is also based on a relationship between the soils shear modulus and the square root of the mean stress. Experimental data on a 0.15 m diameter (Fig. 23) shows the usefulness of this relationship for predicting permanent displacements for model tests performed at mean vertical loads ranging from 100 to 800 kN.

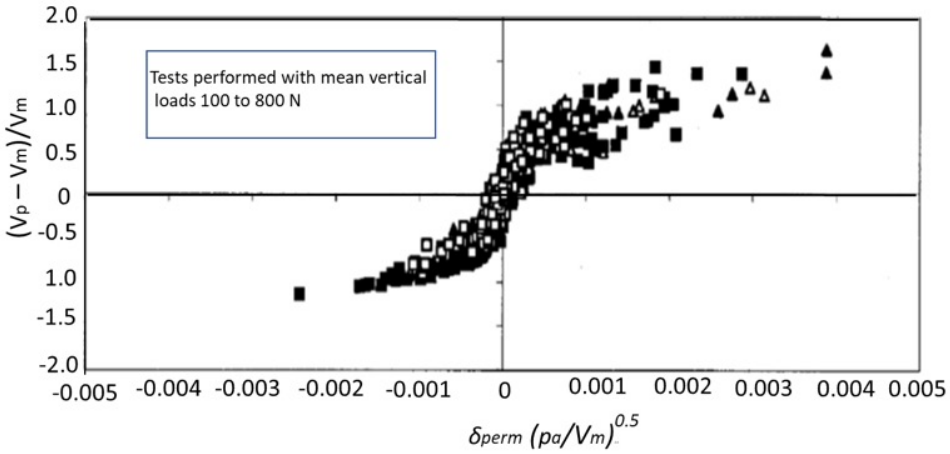


**Fig. 23. Normalized permanent displacements (from Byrne and Houlsby 2002)**

Nielsen et al. (2017) also note that the total reverse end bearing results from a combination of dilative nature of the sand and the 'suction effect' from the pore pressure response. They further note that small scale tests of sand prepared at the same densities but with smaller stress levels will have a greater tendency to dilate, thereby potentially increasing the reverse end bearing stresses above those available at higher stress levels.

Kelly et al. (2006) have proposed scaling relationships to compare model tests at different scales. Based on the normalization procedures they found consistent normalized stiffness values at different scales within individual cycles. However, the cumulative normalized displacements were found to depend on the method of installation. Model tests installed with suction were found to have greater cumulative displacements versus those installed by pushing. Field tests, installed with suction, were found to have significantly less accumulated normalized displacements versus the smaller sized model tests installed with suction.

Finally, based on the results discussed above it appears the ability of a multi-legged structures under tensile loads on sandy soil to rely on reverse end bearing will require additional consideration. More realistic geometries and loads for the prototype cases could provide a basis for taking a more aggressive approach to resisting uplift loads. Kelly et al. (2006) discuss the need for larger scale tests (e.g. centrifuge or large-scale field) to verify designs.

## FATIGUE ISSUES FOR CONDUCTORS AND STEEL CATENARY RISERS IN CLAY SOILS

### *Overview*

The fatigue of conductors or risers depends on the cumulative response of the pipe to a range of loading conditions. While the maximum design load will result in the most fatigue damage/cycle more modest loading conditions will cause more damage because of the larger number of cycles. Clukey et al. (2017) indicate that the most fatigue damage for a Steel Catenary Riser (SCR) occurs from loading events with return periods from ½ to 2 years. Therefore, the soil stiffness required for accurate predictions of fatigue life (inverse of damage) requires knowledge of the soil stiffness at relatively small displacements. In addition, because fatigue damage results after many thousands or even millions of cycles the soil response of

most interest occurs after the soil has undergone both degradation and consolidation. The degradation results from repeated loading with reductions in stiffness while consolidation results in an increase in stiffness over time. With subsequent loading degradation can occur again with additional reductions in stiffness.

The following two approaches can be used to define the soil stiffness throughout the life cycle:

- Describe the soil-structure interaction (SSI) from the time immediately after the installation and track the change in stiffness from the degradation and consolidation effects. This approach is perhaps more appropriate for extreme loading events where the most severe stress conditions in the soil are realized for the first time.
- Focus on degraded soil conditions after the soil has reached steady state conditions. This approach overlooks the complex transient part of the loading and assumes that the number of cycles for the soil to reach steady state conditions is small compared to number of cycles contributing to fatigue. This approach, however, does not explicitly consider the potential interactions between load levels for random loading events or potential consolidation effects. Nonetheless, the methodology is easier to implement and can be checked by comparisons with measured data converted to fatigue (http://www.am.chalmers.se/~anek/teaching/fatfract/98-4.pdf) through Miner-Palmgren techniques.

The two fatigue examples discussed below have used this later approach.

### *Conductor Fatigue*

As discussed by Jeanjean (2009) the fatigue of conductors is often an issue for the first threaded connection, usually located about 10 m below the mudline. The lateral stiffness of the soil is an important part of the overall fatigue assessment. Nonlinear soil springs (p-y curves) for piles have often been used to characterize the soil stiffness. The existing p-y curves for piles in API RP 2A (2007) were developed in the 1960s when the primary concern was the lateral resistance of piles to support jacket structures under severe storm loading conditions. The concern was not about fatigue at lower load levels. Therefore, it is reasonable to expect that the p-y curves for piles may not provide good estimates for fatigue loading.

To better determine the appropriate soil stiffness for the fatigue of conductors the API p-y curves were re-examined with both 3-D finite element analyses and centrifuge model testing (Jeanjean 2009). Example comparisons between the finite element results, centrifuge data and API curves are shown on Fig. 24.

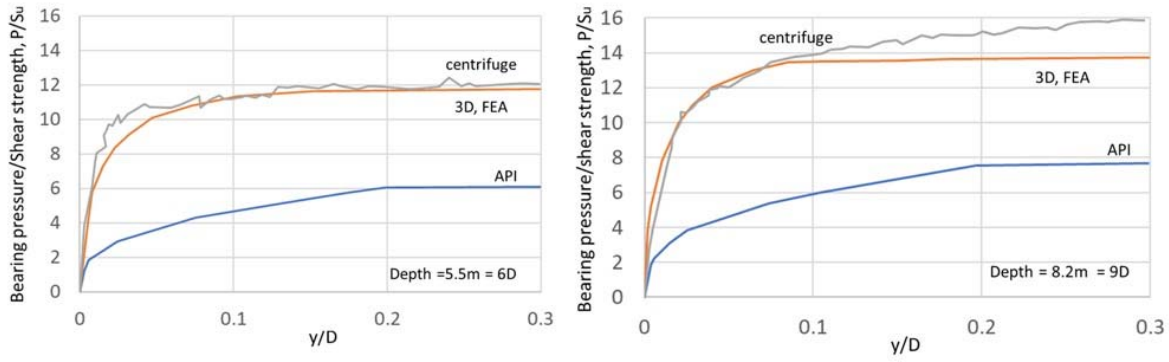


**Fig. 24. Comparison of API recommended backbone lateral resitance cuves versus 3D FEA and centrifuge results (modified from Jeanjean 2009)**

Both the finite element and centrifuge results show that the API curves underestimate both the initial stiffness and the ultimate resistance. Although the agreement between the finite

element and centrifuge results is encouraging, two additional comments should be made. First the curves in Fig. 24 represent backbone curves for the initial loading. The more appropriate stiffness for fatigue is an unload-reload curve that can be substantially stiffer than that derived from backbone curves. Secondly after many cycles of undrained loading, the p-y curves will degrade, reducing the soil stiffness. The unload-reload effect and the cyclic degradation will therefore be compensating.

Many software programs utilize the backbone curve to perform modal analysis for fatigue assessments. Once the various displacements modes are estimated the fatigue damage is then calculated by using the tangent stiffness along the backbone curve. Jeanjean (2009) has noted that based on the centrifuge results the fully degraded unload-reload stiffness was always greater than the tangent stiffness on the backbone curve at comparable load levels. Therefore, the use of backbone curves is conservative for fatigue assessments below the seafloor since stiffer p-y springs reduce curvature and moments below the mudline.

Based on the centrifuge and finite element results discussed above Jeanjean (2009) developed the following revised backbone p-y formulation:

$$\frac{P}{P_{max}} = \tanh\left\{\frac{G_{max}}{100S_u}\left(\frac{y}{D}\right)^{0.5}\right\} \quad [22]$$

Where:

$$P_{max} = N_p S_u \quad [23]$$

$N_p$ is a bearing capacity factor which varies from 8 at the seafloor and has a limiting deep value of 12, $G_{max}$ is the maximum shear modulus, $S_u$ is the undrained shear strength, $y$ is the displacement and $D$ is the diameter. For a typical value of $G_{max}/S_u$= 500, the above curves are similar to those in the updated framework of Jeanjean et al. (2017) for soft clays if no gapping is assumed.

Jeanjean used this revised formulation to predict the fatigue life of the conductors tested in the centrifuge. Comparisons between predictions made using the API criteria and this formulation are shown on Fig. 25. Also shown on this figure are the 'measured' fatigue life profiles based on strain gauge measuremment in the centrifuge tests.

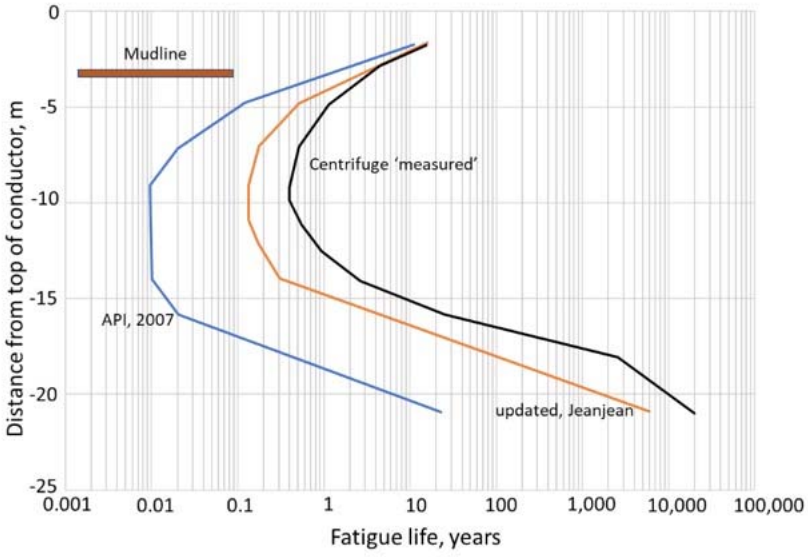


**Fig. 25. Comparison of fatigue life profiles for API, updated Jeanjean (2009) and centrifuge**

At the depth (3 to 11 m below mudline) of the lowest fatigue life, the API p-y curves underpredict the fatigue life by as much as a factor of 100. The p-y curves based on the Jeanjean modifications are in much better agreement with the measured data, but still underpredict fatigue life by about a factor of 3 to 4 in the most critical depth range. As discussed above, this underprediction is due to the use of the tangent stiffness along the backbone curve.

Zakeri et al. (2015) performed an additional series of tests and focused on the fully degraded unload-reload secant stiffness to derive the appropriate soil stiffness for both random and harmonic loads. Based on all the test results they derived the following equation for the normalized secant stiffness.

$$K_{\sec\_ss\_Norm} = 0.67\left(\frac{y}{D}\right)^{-0.97} \quad [24]$$

Where the normalized secant stiffness, $K_{\sec\_ss\_Norm}$ at the steady state degraded condition is the normalized force, $P/(N_p S_u)$, divided by the normalized displacements, $(y/D)$. The bearing capacity term, $N_{p,}$ is as defined by Jeanjean (2009). The force, $P$, and the displacements, $y$, were determined from the strain gauge/moment data collected during testing by evaluating the second derivative and second integral of the moment profile, respectively.

It should be noted that by de-normalizing the force and displacement data, p-y curves can be constructed for various depths and conductor diameters. While such curves would look similar to the previous derived backbone curves, they fundamentally are an assemblage of data where each point represents the secant stiffness after cycling to the steady state condition at a particular load or displacement. The effectiveness of using the steady state secant stiffness to evaluate fatigue can be best evaluated by comparing the measured fatigue from the centrifuge tests to the predicted values using Eq. 24.

Fatigue results obtained by Zakeri et al. (2015) using the above approach are shown on Fig. 26. The curves show the normalized fatigue life versus depth where the normalized fatigue life is normalized by the lowest fatigue life from the centrifuge test results. The '$K_{\sec\_ss}$ no damping curve' are the predictions using the stiffness values described above. The other two curves represent fatigue predictions using the same stiffness values but including soil damping in the formulation. Procedures for including the damping are described in Zakeri et al. (2015).

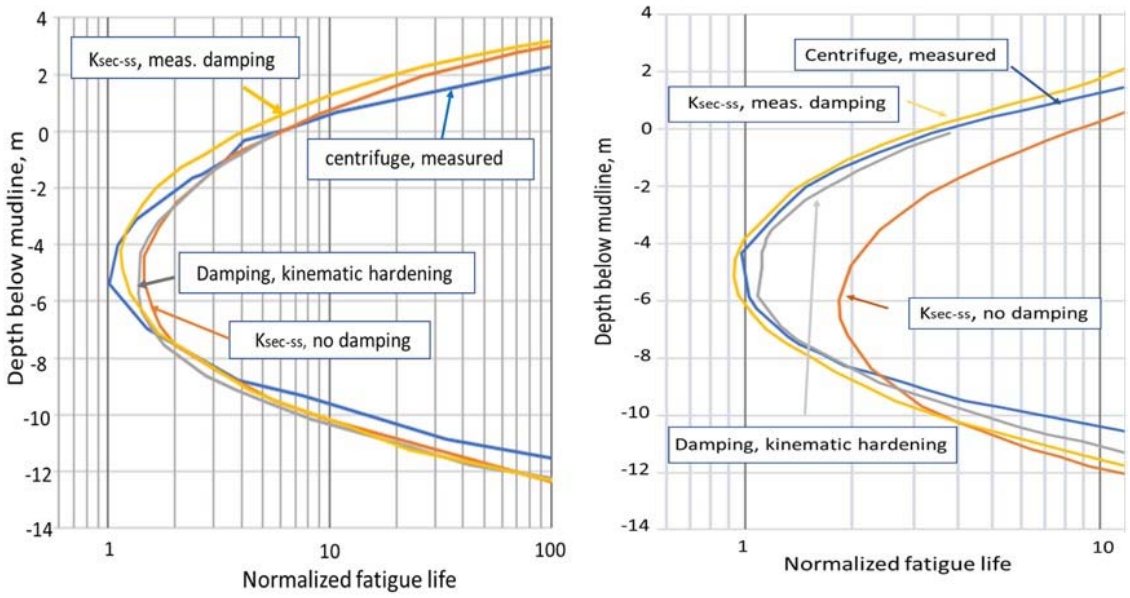


(a) (b)

**Fig. 26. Comparison of conductor fatigue results for (a) harmonic and (b) random motions (from Zakeri et al. 2015).**

Figure 26a shows results for harmonic loads with a one-way amplitude of motion of $0.025D$. Figure 26b shows results for random motions. The results for the harmonic motions show very good agreement between the measured fatigue life and the three predictive methods described above, although the results which include damping appear slightly better. The predicted results are generally within ±20% within the depth range with the lowest fatigue life and is generally very good throughout the entire profile.

Figure 26b, however, suggests that the inclusion of damping improved the predictions. The agreement between the predictions with damping are similarly as good as those for the harmonic data (Fig. 26a). However, the predictions only using soil stiffness appear to slightly overpredict the fatigue life. At the most critical depth this difference is about a factor of 2 which is relatively small considering that fatigue life varies with about the third power of the stress level.

It is interesting to note that without the inclusion of soil damping the predicted fatigue in Fig. 26b results in greater fatigue life than either the experimental results or the predictions which include damping. This observation is somewhat counterintuitive since damping tends to provide an additional transient restraint which would tend to restrict curvature and displacements. A possible explanation for this observed behavior is that the tests were performed with displacement control at the top of the conductor pile. While the inclusion of damping may have provided more resistance in the soil, this added soil resistance from damping for a given displacement would produce more curvature toward the top of the pile and a reduced fatigue life. This appears to be the case where, as shown on Fig. 26b, the divergence between the fatigue life for cases with and without damping occurs in the top 8 m. Below 8 m the predictions with and without damping appear to be similar.

The importance of the type of loading, either load or displacement control, will also have an important effect on the fatigue results for Steel Catenary Risers (SCRs). The next section will highlight how experimental model testing has added to understanding SCR fatigue response.

### *Steel Catenary Riser (SCR) Fatigue*

Steel Catenary Risers are an attractive option for deepwater facilities, with significant potential costs savings versus other riser options. However, one key aspect regarding their feasibility involves the fatigue life of the riser system. The two most critical areas for fatigue occur at the hang-off point where the riser departs from the facility and the touchdown point at the seafloor (Fig. 27). Fatigue at the touchdown point depends significantly on SCR-soil interaction.

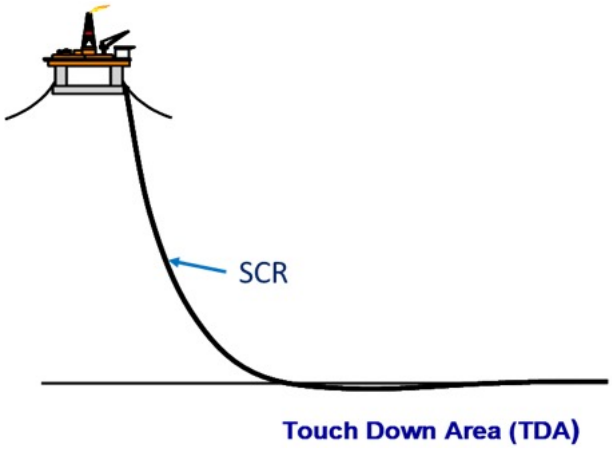


**Fig. 27. Schematic of SCR and Touchdown Area**

Although substantial work has been done to characterize the SCR-soil interaction, many of the approaches developed have relied on simple linear-elastic soil models or more complex models (Bridge et al. 2004; Aubeny and Biscontin 2009 and Randolph and Quiggin 2009) with a significant number of input parameters. The overall problem is complicated by:

1. The loads at the touchdown point result from heave, surge or sway motions. These loads have both low frequency currents and vessel motions as well as higher frequency components from waves and vortex induced vibrations.
2. The soil most impacting fatigue is in the upper few meters which typically has a higher strength crust overlying more normally consolidated soils.
3. A significant trench has been observed in the field near the touchdown point, extending to as much as 1 to 2 m or more below the seafloor. This trench is formed by both the mechanical pipe-soil interaction and an erosional process from high water velocities from the pipe moving inside the trench.
4. The movement of the pipe can result in significant degradation of the soil stiffness. In between loading events the soil can consolidate and regain stiffness.

Model testing has been used extensively to determine the soil response. Some of the initial tests were performed by SINTEF (2001) and Bridge (2005). These tests were part of a Joint Industry Project (JIP) performed on short pipe sections with vertical motions and are referred as segment tests. In these tests, as the loading amplitudes and cycles increased, the soil stiffness significantly degraded. Other tests were performed as part of the STRIDE JIP in about the same time frame (Willis and West 2001) where a truncated section of a riser was tested in Watchett Harbor, UK (Fig. 28a). These tests had a loading frame on a dock and a 15.4-cm (6-in.) riser section that extended out into the harbor. The results from these tests, which are referred to as sectional tests, likewise showed a significant reduction in soil stiffness with increased displacements and cycles.

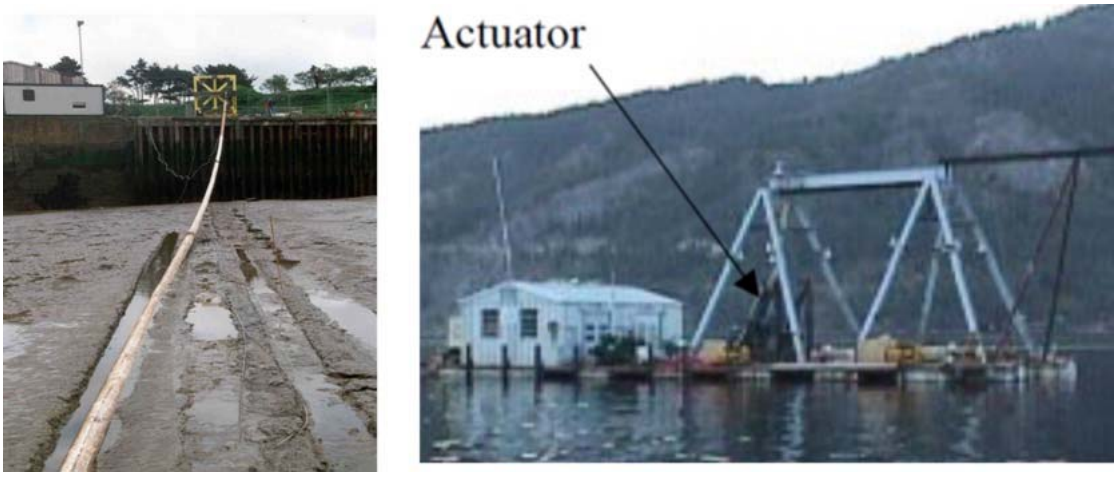


(a) (b)

**Fig. 28. Sectional tests in (a) Watchett harbor and lake tests in (b) Lake Oreille Oregon (from Grant et al. 1999)**

Other field model tests were performed on a 7.6-cm (3-in.) diameter pipe in Lake Oreille, Oregon (Grant et al. 1999; 2000) where the riser was loaded with heave motions from a barge (Fig. 28b). These tests showed that, in addition to high moments at the touchdown point, equally high moments were observed at the 'hogback' location where the pipe curvature reversed prior to transitioning into the flowline.

The CARISMA and STRIDE tests formed the basis for an initial hyperbolic nonlinear soil model (Bridge 2005 and Bridge et al. 2004) which highlighted many of the important features required for a nonlinear model. Aubeny and Biscontin (2009) and Randolph and Quiggin (2009) further refined this approach and developed nonlinear models capable of tracking the pipe penetration into the soil with repeated load cycles. The Randolph and Quiggin model has been implemented into a commercial software code.

Motivated by the need to better understand the cyclic behavior of the pipe-soil interaction and the trench formation Clukey et al. (2005) performed additional segment tests. They observed that:

- For tests with no uplift and normalized vertical displacements ($z/D$) of 0.0003 to 0.002 the steady state normalized soil stiffness, $K = k/N_c S_u$ varied between about 200 and 320. These bracketed the predicted normalized stiffness values ($K$=270) cited by Bridge et al. (2004) for initial small displacements and suggested that there was negligible cyclic degradation at these displacement levels.
- For tests with some uplift and $z/D$ ratios from 0.002 to 0.02 the normalized stiffness ($K$) degraded to about 100 after about 300 cycles.
- As the level of cyclic loading increased to $z/D$ values of 0.01 to 0.03 with some uplift the normalized stiffness values ($K$) further decreased to a range of 25 to 70 after several hundred cycles loading. In one of these tests the loading was stopped overnight and commenced the following day. The initial normalized soil stiffness increased to about 100 after the overnight wait but then decreased in a few hundred cycles back to the lower values observed the previous day.
- Finally, for tests with enough uplift to cause separation of the pipe from the soil ($z/D$ of 0.04 to 0.05) the normalized stiffness ($K$) decreased substantially to values ranging from less than 1 to about 8 after several tens to a few hundreds of cycles of loading.

Based on the results from this series of tests the following equation was derived for the steady state secant stiffness:

$$\frac{k}{N_c\, S_u} = 0.37\left(\frac{z}{D}\right)^{-0.94} \quad [25]$$

Where $k$ is the degraded steady state stiffness and $N_c$ is the bearing capacity factor (~6 to 8). At small displacements ($z/D$<0.001) the normalized soil stiffness is assumed constant at 250.

Following these segment tests and based on the scarcity of field data and the need to consider interactions along the SCR, additional sectional centrifuge tests were performed (Elliott 2013). To perform the tests a container box about a 3 m long was fabricated (Fig. 29).

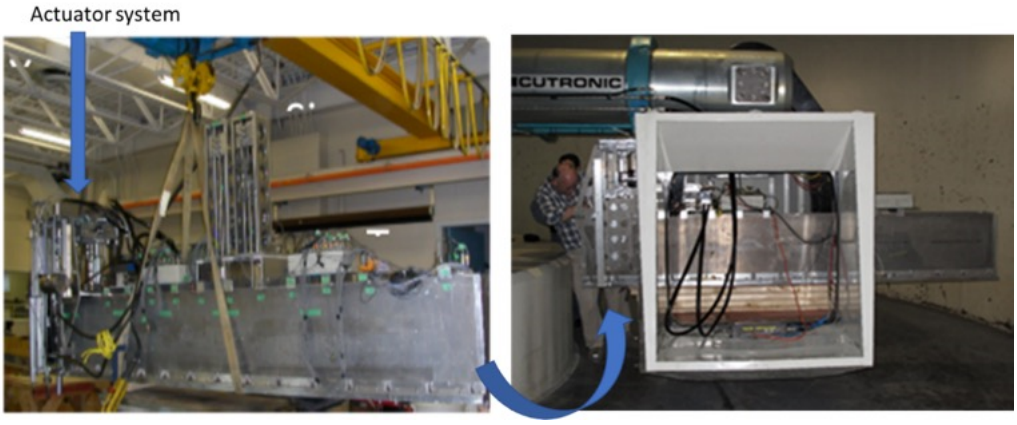


**Fig. 29. Long box being lifted after consolidation and placed onto centrifuge platform.**

This long box allowed testing SCRs with prototype lengths of about 110 m and pipe diameters of 0.30 m and 0.51 m (12 and 20 in.). Initial tests were performed on both kaolin and GoM clays. Both heave and surge motions at low and high frequencies (0.05 Hz and 1 Hz model frequencies) were applied for 1-yr winter storm conditions. The loads were applied at a prototype mean position about 5 m above the mudline.

Numerical analyses (Bhattarcharyya et al. 2011) confirmed that this load point was sufficiently away from the touchdown point to not significantly influence the results. Initially 60 cycles and 1,200 cycles of the 0.05 and 1 Hz respectively loadings were applied for the 1-yr. winter storm condition. The results from this test (Clukey et al. 2011) for GoM soil are shown on Fig. 30.

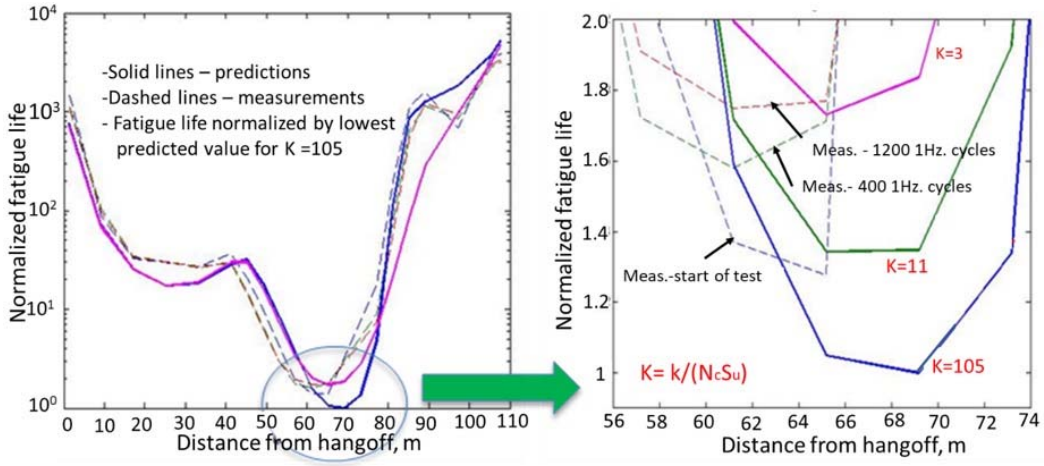


**Fig. 30. Fatigue results for Gulf of Mexico clay on 0.51 m diameter SCR. (modified from Clukey et al. 2011)**

Also shown on Fig. 30 are numerical simulations for dimensionless spring constants ($K$) of 3, 11 and 105. In this figure the results are normalized by the lowest predicted fatigue life for the

$K$=105 stiffness case. The experimentally based measured fatigue results show that for the first cycle of loading the normalized stiffness, $K$ , is between 11 and 105 (about 20) at the most critical fatigue point when compared to the predicted results. After the first 400 cycles the normalized stiffness from the measured results reduced to between 3 and 11 (about 6) and with 1,200 cycles the measured normalized stiffness reduced to about 3. There also is about a 3 to 4 m shift versus the numerical predictions in the location of the critical fatigue point.

To extend the results shown on Fig. 30 for GoM clays, recognizing that each point along the SCR will have different stiffness values depending on displacement levels, the data obtained from the segment tests described above were used as a starting point for a sensitivity analysis to develop a nonlinear model. To do this sensitivity analysis the power law regression curve (Eq. 25) was used to analyze the fatigue for the data described in Fig. 30. In addition, a series of four sensitivity curves were generated with different initial stiffness values and asymptotic peaks i.e., coefficients varied for the power law fit.

Three of the 5 curves tested provided a very good fit to the data (Clukey and Zakeri 2017) when the experimentally based measured fatigue results were shifted 3 m to account for the offset observed in Fig. 30. As discussed by Clukey and Zakeri (2017) the predicted results showed good agreement for the entire fatigue profile and were within ±15% in the most critical fatigue region.

An average was then taken of the three best power law fits and this average was then transformed into the following hyperbolic nonlinear soil model for GoM clays:

$$\mathrm{Q_n} = \frac{\mathrm{Z_n}}{(\mathrm{A'}+B'\mathrm{Z_n})} \quad [26]$$

$$\mathrm{A'} = \frac{(1-\mathrm{X})\mathrm{Z_{nu}}}{\mathrm{Q_{nu}}} \quad [27]$$

$$\mathrm{B'} = \frac{\mathrm{X}}{\mathrm{Q_{nu}}} \quad [28]$$

Where, $Q_n$ is the normalized force, $Q/(N_c S_u D)$, $Z_n$ is the normalized displacement $(z/D)$, $X$ is a curve fitting parameter (approximately 0.85 to 1.0), $Z_{nu}$ is the normalized displacement at $Q_{nu}$, which is the normalized peak force. The parameters $X$, $Z_{nu}$, and $Q_{nu}$ can be selected to provide the best fit to the averaged power law results. The values selected for $X$, $Z_{nu}$ and $Q_{nu}$ were 0.96, 0.10 and 0.35, respectively.

A similar approach was used to evaluate sectional centrifuge test results on offshore Angolan soils. For these tests the segment $1g$ test results performed by Aubeny et al. (2015) for 100 cycles of loading were used directly as the basis for the pipe-soil response. Once again input motions to simulate 1-yr. loading conditions were used in the centrifuge tests for a prototype pipe diameter of 0.31 m (12 in.). The comparisons between the measured fatigue and the predicted fatigue using the Aubeny et al. data are shown on Fig. 31.

The parameters for $X$, $Z_{nu}$, and $Z_{nu}$ for deepwater Angolan soil to be used in Eq. 26 to Eq. 28 are 0.98, 0.10 and 0.13, respectively. The agreement between the predicted results using the non-linear soil model and the measured fatigue for the centrifuge is very good with the centrifuge able to capture the critical point at about 50 m from the hangoff load point. Overall the agreement between measured and predicted valuses is about ±20%.

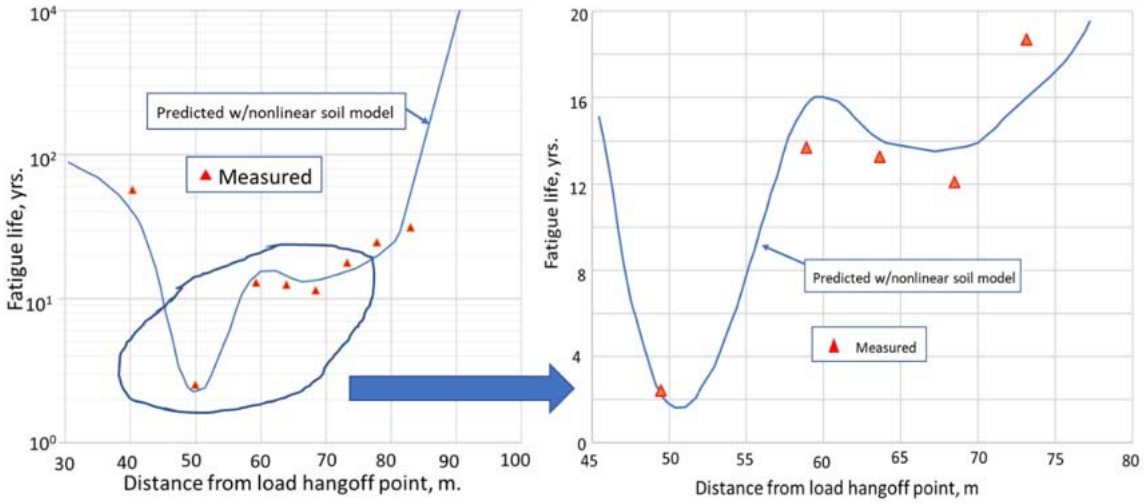


(a) (b)

**Fig. 31. Comparison of measured versus predicted fatigue with non-linear soil model for Angolan deepwater soil (from Clukey and Zakeri 2017).**

Another issue regarding soil-pipe interaction on SCRs is the impact of the trench underneath the touchdown region. Analytical results on the trench impact have been mixed with some initial studies showing almost a twofold reduction in fatigue life (Shiri and Randolph 2010). More recent investigations, however, have shown more variable results (Randolph et al. 2013) depending on vessel offset position, metocean and soil conditions, and the model used to make predictions. Based on these more recent results the range on fatigue life for the trench case versus a flat seafloor condition was about -25% to +600% while the dominant number of cases analyzed (11 of 29) indicated an increase in fatigue life from 0 to 50% versus a flat seafloor.

As noted, part of the trench formation is caused by an erosional process from high water velocities. The water velocities in the centrifuge sectional tests were not scaled properly and as a result, the maximum trench depths in the centrifuge were much less than trench depths observed in the field. Sectional centrifuge tests were therefore performed (Clukey and Zakeri 2017) on Angolan soil with a pre-cut trench based on trench geometries reported by Bridge and Howell (2007). The maximum trench depth was about 1.04 m with a $z/D$ ratio of 3. The results from the tests on Angolan soil with a flat seabed versus a pre-cut trench are shown on Fig. 32.

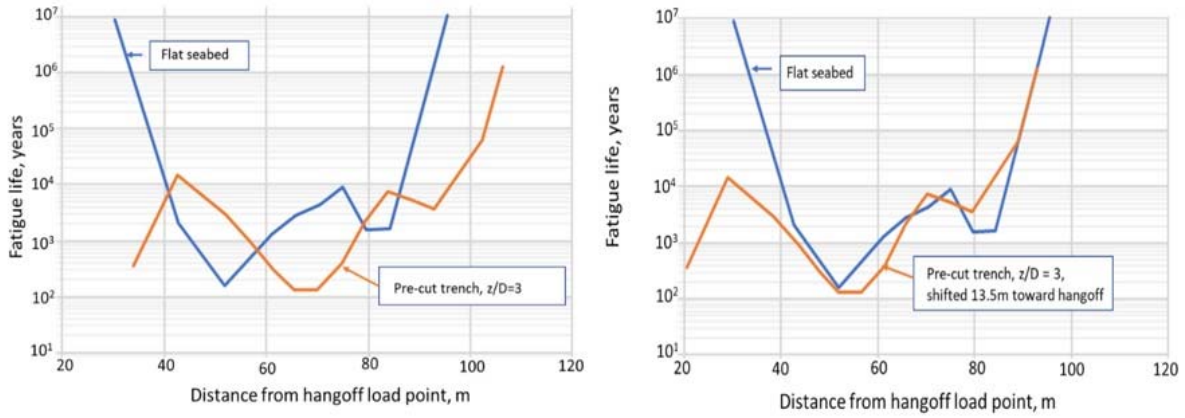


(a) (b)

**Fig. 32. Comparison of fatigue profile for flat seabed and pre-cut trench with maximum depth of 1.04 m (from Clukey and Zakeri 2017).**

The results (Fig. 32a) show the lowest fatigue life with the pre-cut trench is slightly lower (about 20%) than the results with a flat seabed, although the position of the lowest fatigue life is substantially different. If the curve for the test with a flat seabed is shifted about 14 m (Fig. 32b) the two curves match up reasonably well. These observations suggest that as the trench progresses from a flat seabed the critical fatigue point shifts with potentially longer fatigue life for the overall riser. The average Randolph et al. (2013) results for three different trench profiles for the far offset position and GoM soil shows a 2% increase for fatigue life with a trench.

Finally, the impact of long-term consolidation on the soil stiffness (Yuan et al. 2016 and Clukey et al. 2017) has also been demonstrated based on centrifuge tests performed with load control. Figure 33a shows the evolution of the trench and movement of the pipe during two load-controlled tests (10 kPa). On the uplift cycle the 0.6 m diameter prototype pipe was initially displaced about 1$D$ above the bottom of the trench. Figure 33b shows that the stiffness initially decreases due to the remolding process, but then after about 100 to 200 cycles begins to increase due to the consolidation effects.

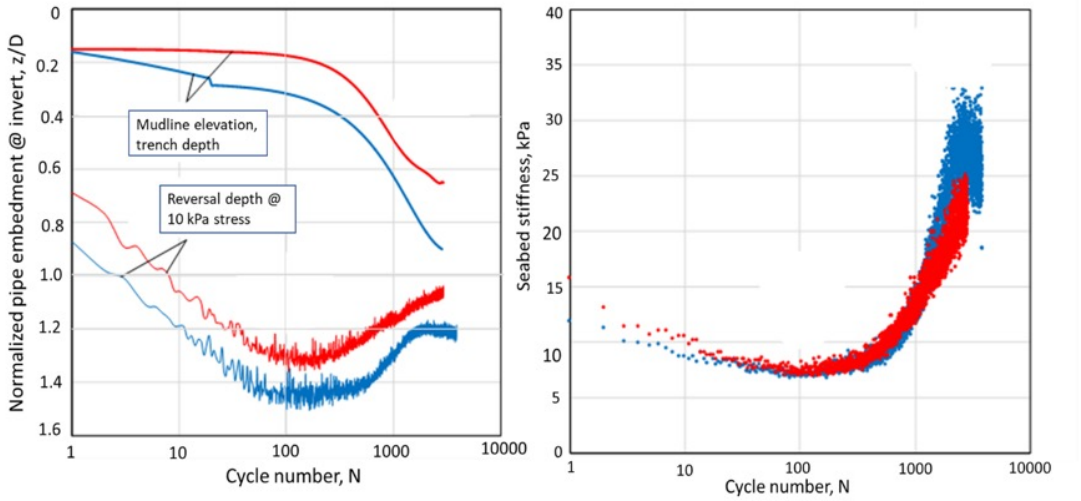


(a) (b)

**Fig. 33. Pipe movement (a) and changes in vertical soil stiffness for load-controlled pipe tests (from Clukey et al. 2017).**

Displacement controlled tests, however, show a different trend. Figure 34 (Aubeny et al. 2015) shows results for a series of tests cycled at 0.05$D$ with wait periods at 200 and 400 cycles, respectively.

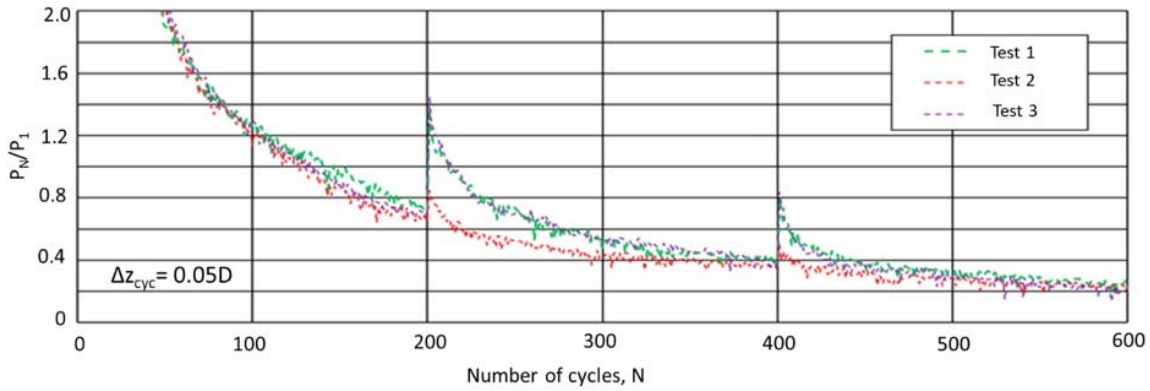


**Fig. 34. Segment tests to investigate cycling and wait period on soil stiffness for SCRs (from Aubeny et al. 2015).**

For Tests 1, 2, and 3 the wait periods were 1 day, 0.2 days and 17 days, respectively. The results show an increase in peak load, $P_N$, normalized by the peak load for the first cycle $P_1$. The ratio represents the change in the secant stiffness for each cycle of loading. After each wait period there is an increase in $P_N/P_1$. For the 0.2 day wait period (Test 2) this increase is relatively small while the 1-day and 17-day wait periods are significantly larger. However, for all 3 tests the secant stiffness degrades again and appears to return to the initial degradation trend.

A possible explanation for the two sets of results could be related to the potential separation of the pipe with the soil during uplift. Clukey et al. (2005) have shown that with displacements of $0.05D$, as per the tests on Fig. 34, or greater, the pipe will likely separate from the soil in uplift. The stiffness degradation that occurred with separation was much more severe than without separation. Therefore, although both the Yuan et al. (2016) and the Aubeny et al. (2015) tests experienced uplift, the Yuan et al. test continued down into deeper and stronger soil less impacted by the separation process. The Aubeny et al. tests were continually in the soil near the bottom of the trench that was highly disturbed and likely experienced high tensile stresses prior to the pipe-soil separation. These tensile stresses and the proximity of the soil to the water at the trench bottom may have caused water entrainment that, after consolidation, reduced soil density and stiffness with further cycling.

## EARTHQUAKE MODELING

### *Overview*

In contrast to onshore earthquake engineering which, in addition to numerical models, benefits from results derived from shake table tests and field observations, offshore earthquake engineering has been mostly limited to results from numerical models. While lessons can be extracted from the onshore experience, there are clearly differences that require consideration. For example, the type of structures, the geological environment and the soil conditions could all impact earthquake response for offshore versus onshore conditions.

One example where differences may occur is the potential liquefaction of sand. Onshore sand deposits have often been subjected to some level of environmental loading where they may have densified to some extent from their initial deposited condition. Because of the densification processes, as a minimum, they may be in a loose to medium dense condition. Although still liquefiable, their liquefaction depth may be limited. Offshore sand deposits, however, can be deposited through turbidity currents that can result in initial densities at or even below the minimum density state (P. Lade, personal communication, 1992). Water depths are also deep enough such that even the largest potential waves will not transfer enough energy to the seafloor to cause densification. Therefore, sand deposits in deep water can be less dense than onshore deposits and may liquefy to greater depths.

To better understand the behavior of offshore structures under earthquake loading, two centrifuge testing programs were performed at the University of California at Davis (UCD). The first program focused on the response of Steel Piled Jacket (SPJ) structures. In this program two separate piles and a single SPJ model structure were tested. The other program tested an offshore manifold supported on four suction caissons and a wellhead structure. The results of these programs helped demonstrate the potential for centrifuge testing to provide much needed data regarding the soil-structure interaction during earthquakes.

It should also be noted that very significant earthquake centrifuge testing facilities exist in Japan. Two of these facilities are owned by two of the largest construction companies (Takenaka and Obayashi) and are mostly used internally to address their own critical design issues (https://www.obayashi.co.jp/en/solution_technology/).

### *Testing Programs*

The centrifuge facility at UCD is shown on Fig. 35. The facility has an 8 m rotor arm (Fig. 35a) and a laminar shear box container (Fig. 35b) that displaces in a simple shear motion along its long axis to reduce boundary effects during shaking. The SPJ was a four-piled structure with 1.52 m prototype diameter piles embedded 24.6 m below the top of soil deposit (Fig. 35c). Additional details on the SPJ structure are provided in Litton et al. (2014).

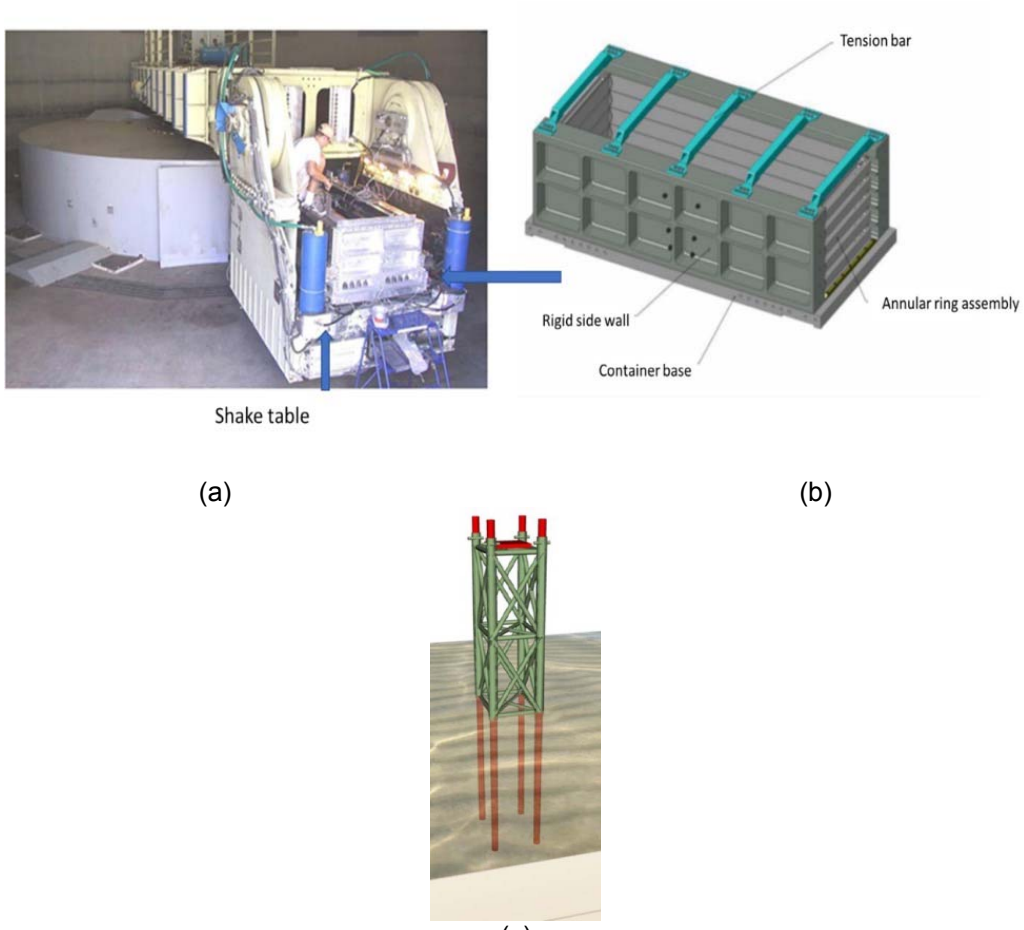


**Fig. 35. UC Davis centrifuge with shake table (a) laminated shear box (b) and schematic of SPJ.**

As noted above, earthquake model testing in a centrifuge must be performed at much higher frequencies to properly simulate inertial conditions. The tests performed at UCD were performed at 58$g$ for both the SPJ and manifold programs. Therefore, the time histories of the input motions were decreased by a factor of 58.

The earthquake motion used in the SPJ program were based on the 1988 Loma Prieta earthquake while the manifold/well head motions were based on the 1994 Northridge earthquake and the 1978 Tabas earthquake in central Iran. Both Extreme Level Earthquakes (ELE) and Abnormal Level Earthquakes (ALE) were performed in each program. ELE events typically represent return periods of several hundred years while ALE events several thousand years.

The soil used in each program was normally to slightly overconsolidated clay. The clay in the SPJ program was kaolin while the clay in the manifold/well head program was a mix of natural clay from the site of interest and kaolin (20% / 80%). Sand layers were placed at the bottom of the deposit for each program to help expedite consolidation. Several additional thin (2 to

4 mm) sand layers were also placed within the deposit for the manifold/wellhead tests due to the lower permeability and slower consolidation of the 20/80 mix. The prototype depths of soil for the SPJ and the manifold/wellhead program were 30.1 m and 27.0 m, respectively. The soil profiles were prepared by consolidation in layers outside the centrifuge. The desired profiles were obtained by varying the vertical stress, depending on the final depth of each layer. Shear strength profiles were determined for both programs with T-bar testing. Additional details of the test preparations, instrumentation and procedures used are provided in (Litton et al. 2014 and Zheng et al. 2015).

### *Steel Pile Jacket Earthquake Study*

To investigate the response of a SPJ under seismic loads the following series of tests were performed:

- Vertically loading a 1.52-m (60-in.) diameter pile at penetration rates from 7 mm/s to about 150 mm/s.
- Step wave-free vibration tests where the shake table was rapidly displaced, stopped and the unforced motions of the bending pile and structure measured to determine the natural period and damping. After about 30 s of unforced motions the displacement was reversed, and the shake table set back to its' original position. Three separate step wave tests were performed with maximum input accelerations of $0.03g$, $0.12g$ and $0.12g$.
- A frequency sweep test where a constant ground acceleration was applied for ten cycles at frequencies of 1.57 Hz, 1.32 Hz, 0.91 Hz, 0.77 Hz, 0.65 Hz, 0.57 Hz, 0.51 Hz. The targeted input acceleration at all frequencies was $0.12g$. The actual input accelerations ranged from $0.25g$ at 1.57 Hz to $0.13g$ at 0.5 Hz.
- A small Loma Prieta earthquake with a maximum input ground acceleration of $0.035g$.
- A large Loma Prieta earthquake with a maximum input ground acceleration of $0.46g$.

#### Rate Effects on Piles

The results from the axial pile test (Litton et al. 2014) are shown on Fig. 36.

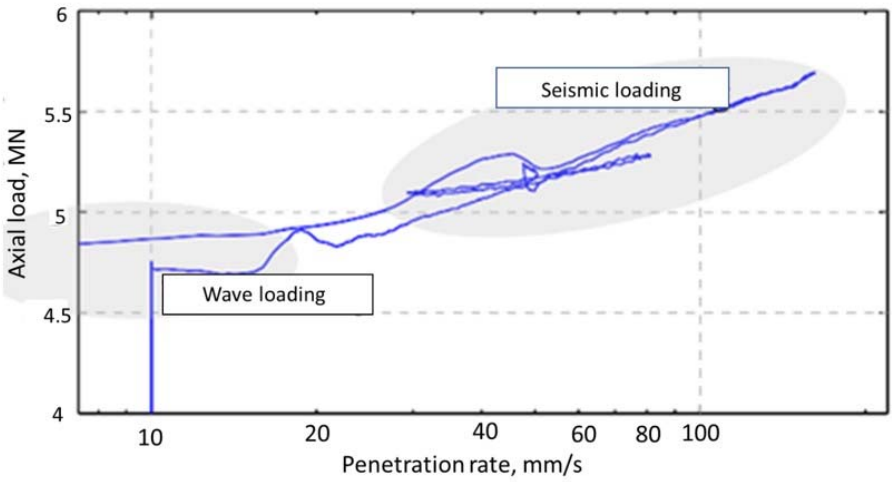


**Fig. 36. Axial pile tests rate effect results for 1.52-m diameter pile (modified from Litton et al. 2014).**

The results suggest about a 13% increase in capacity for penetration rates ranging from 10 mm/s to 100 mm/s, similar to what Bea (1984) recommended per log cycle of loading. Assuming that a typical wave period for a large wave is 15 s versus about 1 s for earthquakes, then the difference in capacity between the wave versus earthquake rate of loading is about

15%. If the static capacity is based on a laboratory test that was performed with a failure time of one hour (3,600 s) then the increase in capacity for the earthquake loading rate (loaded to failure in ¼ cycle) versus the capacity predicted based on the lab tests would be 66%. This is consistent with the 40% increase reported by Bea for static versus wave rates of loading.

It should be noted, however, that viscous rate effects in the centrifuge is proportional to $v/D$ where the velocity ($v$), which scales 1:1, should be divided by the model diameter ($D$) which would make the rate effects higher than shown on Fig. 36.

## Step Wave – Free Vibration Tests

One of the results from the step wave-free vibration tests (Litton et al. 2014) for the 'bending' pile is shown on Fig. 37.

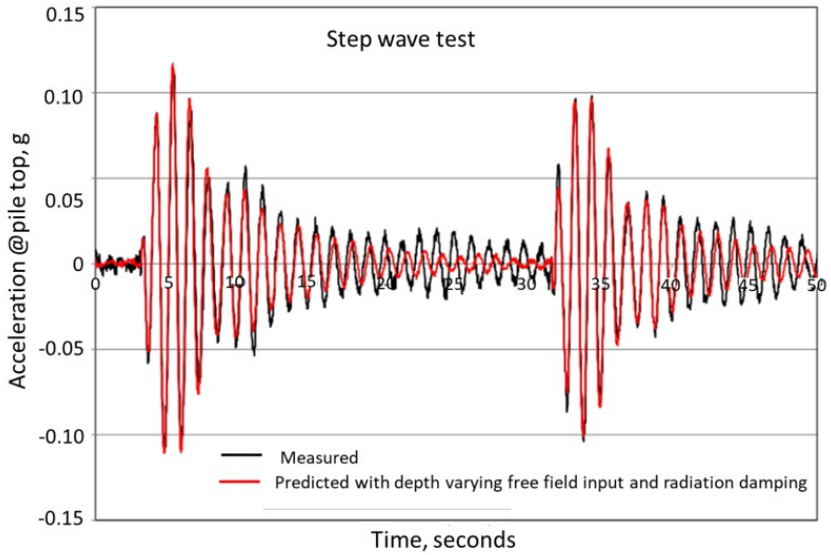


**Fig. 37. Acceleration at top of 1.52-m diameter pile for step wave test (modified from Litton et al. 2014).**

The figure shows the acceleration at the top of the bending pile for both the measured and predicted data when radiation damping and the measured depth varying ground motions based are included in the analyses. The Jeanjean (2009) p-y curves were used in the analyses. The peak values are generally within 5% of the measured values with these assumptions. If radiation damping is not included the predicted peak values were 20 to 50% greater than measured. If both radiation damping and depth varying ground accelerations are not included in the analyses the maximum accelerations were overpredicted by 60% to 90%.

With the results from the step wave test the natural period of the pile and SPJ can be determined. The measured period for the initial step wave experiment for the pile was 1.19 s. Using API p-y curves, the predicted natural period was 1.75 s. Using the p-y curves proposed by Jeanjean (2009), the predicted natural period was 1.14 s. The measured natural period for the jacket structure was 1.0 s.

The damping ratio can also be determined for the step wave tests from the logarithmic decrement of the displacements. The log decrement, $\delta$, is defined as the logarithmic ratio of two successive peaks by the following:

$$\delta = ln\frac{z_1}{z_2} = \frac{2\pi D}{\sqrt{1-D^2}} \quad [29]$$

Where $z_1$ and $z_2$ are the amplitudes of successive peaks and $D$ is the damping ratio.

The damping was evaluated by considering 10 wave cycles and plotting the natural log of the amplitudes versus the cycle numbers. A linear regression curve was then fit through the data and the maximum and minimum values determined to evaluate $z_{max}$ and $z_{min}$. The log decrement was then determined by:

$$\delta = \frac{1}{N} \Sigma \, ln \frac{z_{max}}{z_{min}} \quad [30]$$

Where $N$ is the number of cycles considered. The values of the damping ratios at the $0.03g$ and the two $0.12g$ input accelerations were 2.8%, 4.5% and 4.4%, respectively. The larger values for the final two tests are likely the result of increased material damping at the higher acceleration levels.

Results from the SPJ for the small Loma Preita earthquake indicated that the best match with predictions was obtained with the Jeanjean (2009) p-y curves, full horizontal radiation damping, but only 50% of the vertical radiation damping, suggesting interaction effects between the two components of radiation damping.

## Frequency Sweep

The results from the frequency sweep tests (Chen et al. 2016) are shown on Fig. 38. Both the measured axial pile capacity from the axial pile test data discussed above and back analyses of the pile forces for cases with and without radiation damping are shown. The jacket plunged about 0.48 m (1/3 pile diameter) on the third loading packet (Litton et al. 2014) when the excitation frequency was 0.91 Hz, about the natural frequency of the SPJ measured in the step wave excitation (1.0 Hz).

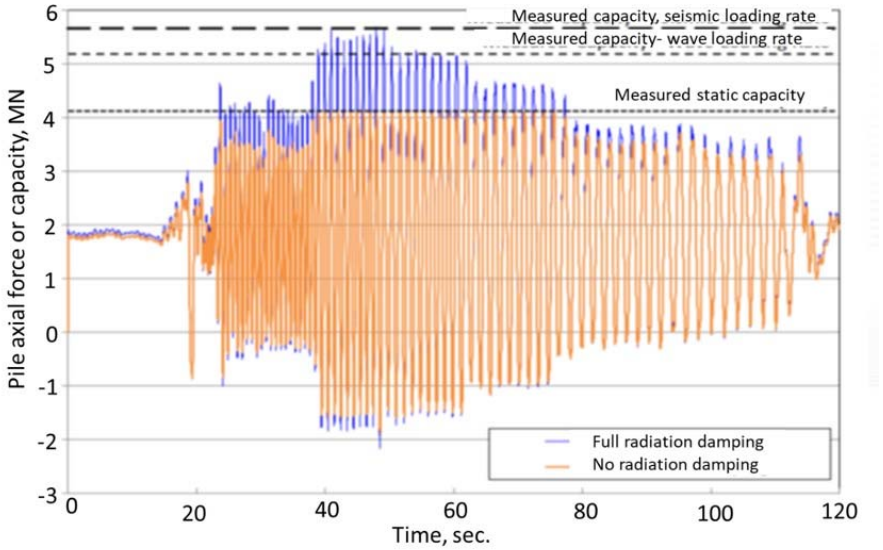


**Fig. 38. Results from frequency sweep test on SPJ (modified from Chen et al. 2016).**

As shown on Fig. 38, the seismic force generated when full radiation damping was included in the analytical model equaled the measured capacity when rate effects for seismic loading are included.

## Free Field Accelerations

For the small Loma Prieta earthquake, the input acceleration from the shake table was $0.035g$ (lower than actual ELE). From 7.6 m below mudline (BML) to 30 m BML (input depth) the peak ground acceleration remained within a narrow range from $0.033g$ to $0.036g$. However, at 3.9 m BML the peak ground acceleration increased to $0.042g$.

For the large Loma Prieta ground motions, the input ground motion was significantly attenuated (Litton et al. 2014) as shown on Fig. 39. On this figure the response spectra at different depths BML are shown on the left-hand side while the time histories at different depths are shown on the right-hand side with the peak ground accelerations listed.

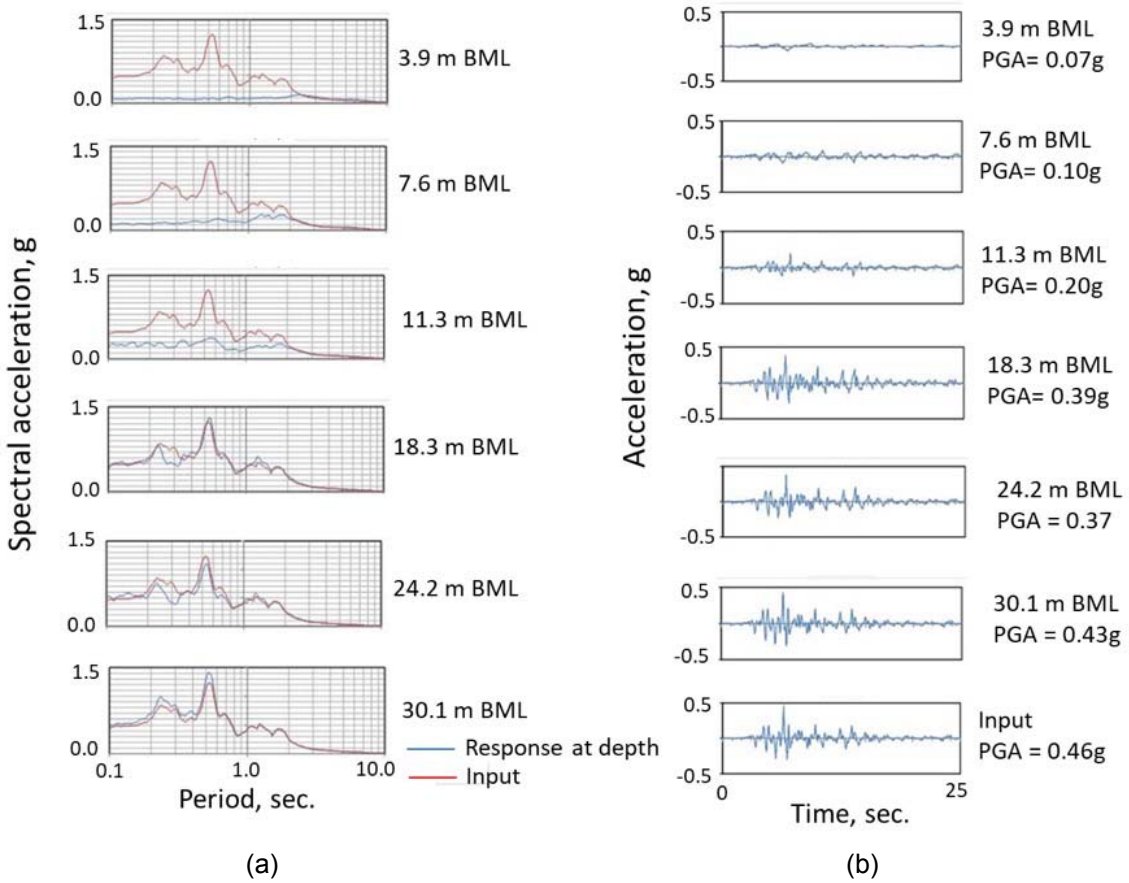


**Fig. 39. Response spectra (a) and time histories (b) for free field accelerations (modified from Litton et al. 2014).**

The peak input acceleration is 0.46$g$. From 18.3 m to 30 m BML the peak ground acceleration remains within a fairly narrow band from 0.46$g$ to 0.37$g$, decreasing to 0.20$g$ at 11.3 m BML and further deceasing to 0.07$g$ at 3.9 m.

Since the pile length was about 24.6 m BML, the ground motions and forces for the top half of the pile would be significantly attenuated based on these results.

A comparison between input motions and near surface ground motions is shown on Fig. 40. The Dickenson (1994) data (field measured Loma Prieta and MARDES ground response analyses) shown on this figure are for soft-medium stiff cohesive soils for the Loma Prieta earthquake. It generally appears that the Dickinson results suggest higher near surface motions compared to the measured data in the centrifuge tests and the Idriss et al. (1976) predictions.

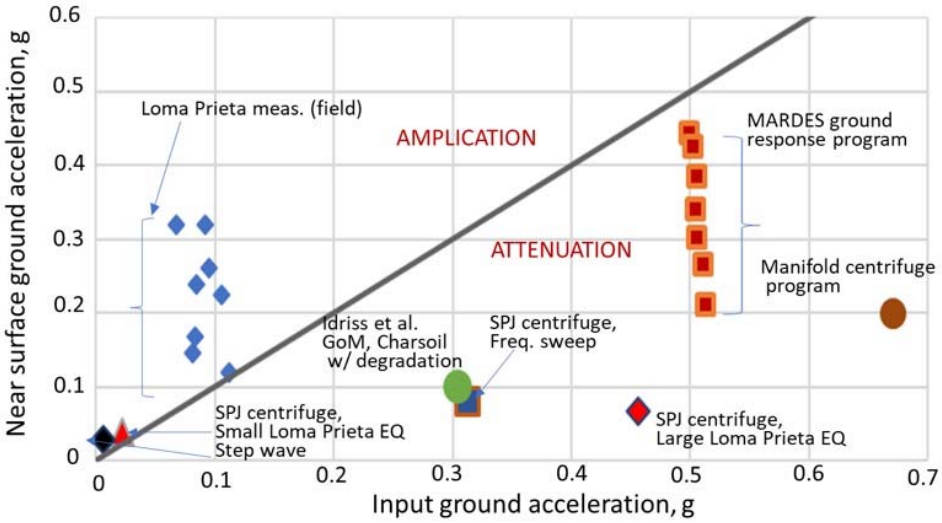


**Fig. 40. Comparisons of input versus near surface ground accelerations (modified from Litton et al. 2014).**

The Idriss et al. response model accounts for changes in in soil strength and stiffness throughout the time history of motion. The soil (GoM clay) considered was a normally consolidated clay with input motions at 61 m and the shallow ground motions at 8.4 m.

The results from the two centrifuge testing programs appear to be consistent with Idriss et al. analyses. The centrifuge results, however, for the large Loma Prieta earthquake may have been influenced by the frequency sweep test which was run first. However, the consistency of the results and agreement with the Idriss et al. analyses suggest that the impact of the frequency sweep test may have been relatively small.

The normalized accelerations versus depth are shown on Fig. 41 for the centrifuge results with input accelerations greater than 0.3$g$ and the Idriss et al. (1976) predictions. Some of the measured accelerations in the centrifuge at the bottom of the clay deposit varied slightly from the acceleration measured on the laminated shear box just below the soil. Therefore, the normalized values were not always 1.0. The results suggest a significant reduction in the free field acceleration for clay layer thicknesses from about 25 m to 60 m (based on the data discussed above) and input accelerations greater than 0.30$g$.

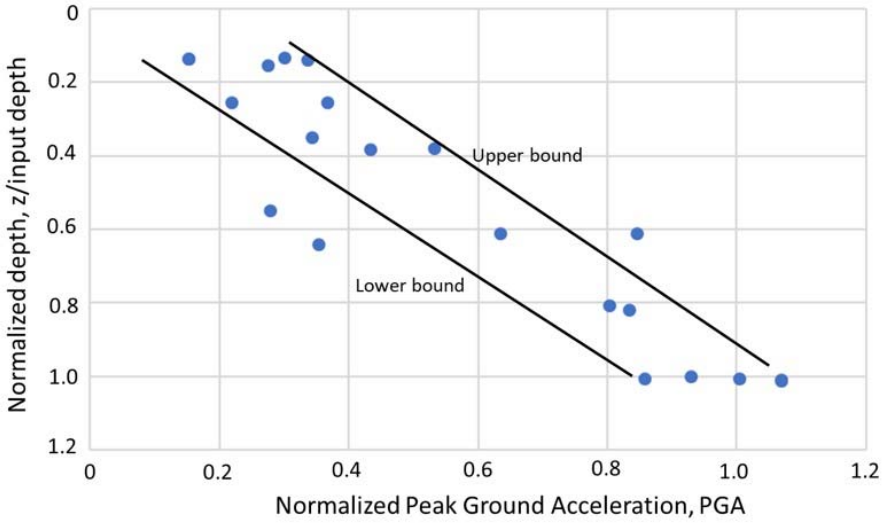


**Fig. 41. Normalized PGA versus normalized depth from centrifuge tests and Idriss et al. ground response analyses – normally consolidated clay with input PGA>0.3$g$.**

Pile Moments and Settlements

Bending moments were determined for the bending pile for the initial step wave test (Fig. 42) where the maximum input acceleration was 0.03$g$. The lateral soil springs were modelled with the p-y springs described by Jeanjean (2009). The results show good agreement between the measured and predicted values when depth varying ground motions are included in the analyses. Good agreement was also obtained when full radiation damping was included with depth varying motions (Litton et al. 2014).

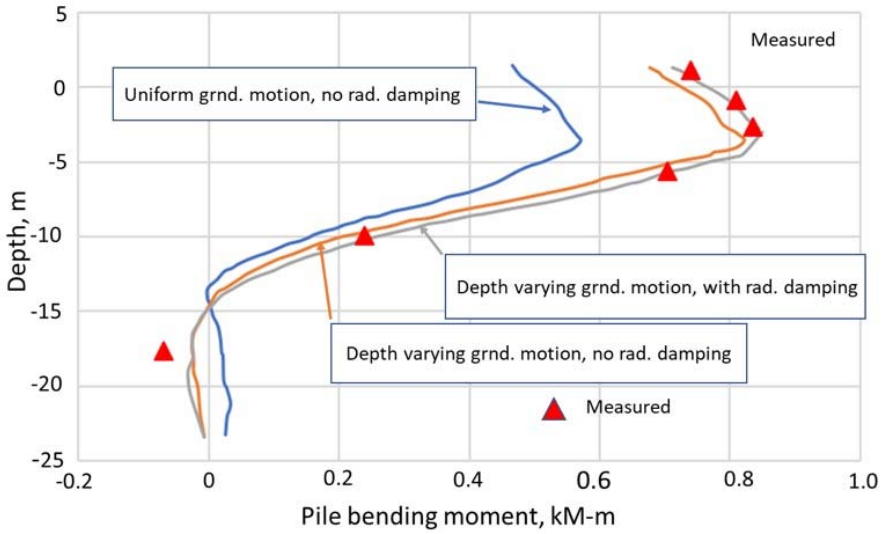


**Fig. 42. Moment comparison for small (0.04$g$) step wave test (modified from Litton et al. 2014).**

Chen et al. (2016) also found good agreement for pile bending moments between a discrete element (p-y and t-z curves) model (CAP 2013) and FLAC3D model which uses a combination of elasto-plastic spring elements to model the interface between the pile and soil and fully non-linear continuum elements to model spatial interactions as well as unloading-reloading behavior and material damping. This comparison was based on a large ALE event where material damping likely dominated the damping response.

As noted, during the frequency sweep test the SPJ structure plunged 0.48 m. The predicted pile settlements using full radiation damping were in very good agreement with the measured settlements. However, for the analyses where no or ½ radiation damping was used the pile settlements were overpredicted with predicted settlements of 0.90 m and 0.75 m, respectively (Chen et al. 2016).

### *Template Manifold Structure Response*

Subsea templates are inherently stable in terms of their global stability. For seismic excitations the critical failure mode is often overstressing the connections due to the relative movements between the manifold and well head. Figure 43 shows the response observed in the model test for the wellhead structure, free field and manifold structure to a large ALE event with a maximum input acceleration of 0.62$g$.

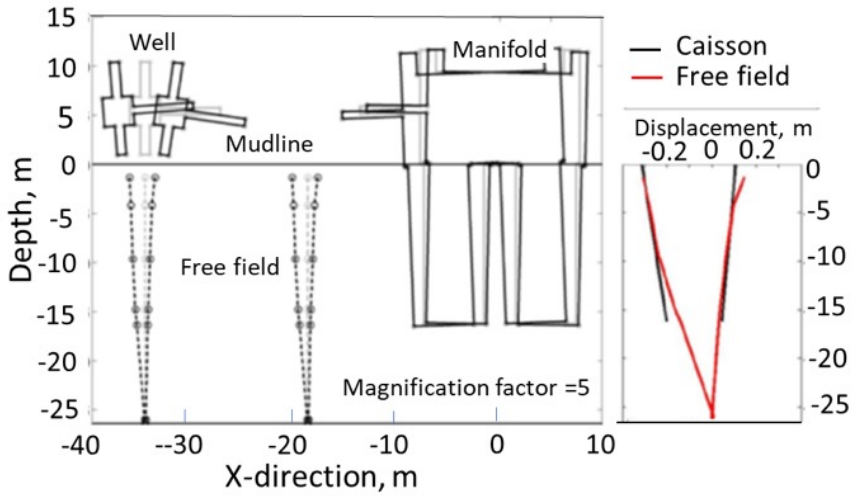


(a) (b)

**Fig. 43. Observed response of manifold, free field and well head (modified from Zheng et al. 2015).**

Figure 43b shows the range of movements for the manifold and free field. The movements at the mudline for both range from about -30 cm to +12 cm. These similar movements suggest small relative displacements between the soil and the manifold. The movements above the mudline where the connections into the manifold occur are about 50% greater.

To determine the stress and moments at the connectors the relative movements between the wellhead and manifold need to be determined. Figure 44 shows these movements at the center of gravity for the manifold and a reference point near the top of the wellhead.

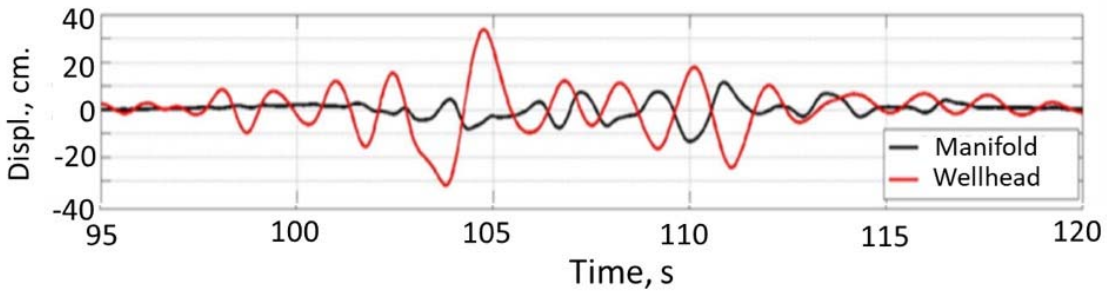


**Fig. 44. Time history of displacements for manifold and wellhead (from Zheng et al. 2015).**

These results together with the data collected to determine the rotations of both these structures provide the information required to determine the stresses and moments at the connector locations.

## CONCLUDING COMMENTS

The paper has described a variety of physical modeling testing programs that have added to the body of knowledge for an array of offshore geotechnical problems. Although some of the tests described may not have satisfied all similitude requirements, they have added critical insights to key issues and helped establish a way forward for future testing and analyses. Centrifuge testing has helped to meet some important scaling requirements, especially the dependence of soil response on stress state. Other parameters, however, may not be met, (e.g. consolidation times and inertial considerations) and appropriate steps should be taken to model these effects as closely as possible, or at least recognize their potential impact on results.

Some of the major lessons learned from the physical model tests highlighted in this paper are as follows:

- Small scale and centrifuge experiments demonstrate the potential for wave-induced shallow failure and/or liquefaction of sand and silts that likely will contribute to sediment scour and erosion and will require more advanced soil mechanics approaches.
- Small scale experiments with a range of Reynold numbers have provided a solid basis for evaluating the impact of debris flows on pipelines.
- Multiple physical model tests of suction caissons in clay that separate side friction from end bearing have reduced uncertainty regarding appropriate design parameters. Small scale (field and lab) tests on suction caissons in sand have highlighted key issues that need consideration as their usage increases in the offshore wind industry.
- Centrifuge testing has helped define the appropriate soil springs required for fatigue assessments of conductors and SCRs. Soil springs based on near or fully degraded soil conditions were shown to agree favorably with measured fatigue results.
- The lack of corroborating data to verify offshore earthquake design procedures makes the use of centrifuge model testing coupled with shake tables to scale inertial effects an attractive option. Some relatively recent tests have shown the need to account for depth varying ground acceleration to accurately predict pile response. Radiation damping further increases the accuracy of predictions, although there may be to be an interaction between the horizontal and vertical damping components. Free field motions from depth to the near surface in normally consolidated clays appear to attenuate faster than onshore data or existing ground response programs suggest.

Finally, physical modeling, as hopefully these examples haved illustrate, offers an attractive option for advancing offshore geotechnical technology and when coupled with other approaches can provide significant advancements to the state of knowledge.

## ACKNOWLEDGMENTS

I would like to begin by thanking the International Society of Soil Mechanics and Geotechnical Engineering (ISSMGE) for inviting me to present this McClelland paper/lecture. It is indeed an honor to follow the four previous lecturers, all of whom I have had the opportunity to work with and learn from throughout my career. We have all benefited from the legacy and inspiration Mr. McClelland provided.

I would also like to acknowledge Professor Armand Silva and Worcester Polytechnic Institute for providing the opportunity to begin working in offshore geotechnics. Professors Fred Kulhawy and Philip Liu of Cornell University are acknowledged for their support and guidance particularly in our efforts to better understand wave-seafloor interaction.

There have been many professional colleagues, too numerous to all name, that have assisted and helped me throughout my career. However, I would especially like to acknowledge some who have helped along the way. Monty Hampton, Dave Cacchione and Hans Nelson of the US Geological Survey, provided lessons and unique opportunities to learn and appreciate the influence of marine geology on our business. Many at McClelland Engineers further enhanced this process. In particular, I have had many enlightening conversations with Alan Young on how integrated studies can best address complex geohazard issues.

My years at Exxon and BP provided numerous opportunities to interact with many who have profoundly impacted my career. Don Murff of Exxon introduced me to centrifuge model testing and more importantly provided an approach to engineering I have tried to follow in my career. Jack Templeton is thanked for his patience and ‘yellow pad’ discussions on many topics related to mechanics and numerical modeling. I have fortunately been able to stay engaged

with both long after our days with Exxon. Philippe Jeanjean of BP is thanked for being a trusted colleague at BP as the company expanded into very deep water regions throughout the world. Arash Zakeri, both while at C-CORE and then BP, has been an inspiration with his hard work.

Various centrifuge facilities and individuals have provided opportunities for me to use this technology on challenging problems. Jacque Garnier (LCPC), Ryan Phillips (C-CORE), Mark Randolph (UWA), Hon Yim Ko (UCB) and Bruce Kutter (UCD) and their excellent staffs and technical support are all gratefully acknowledged for their patience and mentoring.

My partner, Ms.Janis Sanford, is acknowledged for her support and being exposed to far more about engineering than ever imagined or perhaps desired. My two sons, Sean and Kevin, have chosen different paths than their Dad but have been a source of pride for all their hard work and support.

Finally, Mark Randolph, Jack Templeton and Philippe Jeanjean are thanked for their thoughtful comments reviewing the manuscript. Ms. Jill Rivette is thanked for her excellent preparation of the manuscript and making it look very professional.

## REFERENCES

Andersen, K.H., Dyvik, R., and Schrøder, K., 1992. Pull-out capacity analyses of suction anchors for tension leg platforms. Proceeding, Intern. Conf. on Behaviour of Offshore Structures, London, Vol. 1, pp. 1311-1322.

Andersen, K.H., Dyvik, R., Schroeder, K., Hansteen, O.E., and Bysveen, S., 1993. Field tests of anchors in clay II: predictions and interpretations. American Society of Civil Engineers, ASCE J. Geotech. and GeoEnv. Eng, 119 (10), pp. 1532-1549.

Andersen, K.H. and Jostad, H.P., 2002. Shear strength along outside walls of suction caissons in clay after installation. Proceedings, 12th ISOPE Conf., Kyushi, Japan, May.

Andersen, K.H., Randolph. M.F., and Murff, J.D., 2003. Deepwater anchor design practice – phase-II, vol. 2 suction caisson anchors, report to API/Deepstar. Report No. C150, Offshore technology research center, College Station, Texas.

Andersen, K.H., 2009. Bearing capacity under cyclic loading: offshore, along the coast and on land. Canadian Geotechnical Journal, Vol. 46, pp. 513-535.

Andersen, K.H., 2015. Cyclic soil parameters for soil design. Proceedings Intl. Sym. on Frontiers in Offshore Geotechnics, Vol. 1, Oslo, pp. 5-82.

API RP2A-WSD, 2007. Errata and supplement 3 to API recommended practice 2A-WSD recommended practice for planning, designing, and constructing offshore platforms-working stress design. 21st edition, December 2000, Oct.

API RP 2SK, 2005. Design and analysis of station keeping systems for floating structures. Oct., 241 p.

Aubeny, C.P., Han, S.W. and Murff, J.D., 2003. Inclined load capacities of suction anchors. Intl. J. for Numerical Methods in Geomechanics, 27, pp. 1235-1254.

Aubeny, C.P. and Biscontin, G., 2009. Seafloor-riser interaction model. American Society of Civil Engineers, ASCE Intl. J. of Geomechanics, No. 133, May/June.

Aubeny, C.P., White, T.A., Langford, T., Meyer, V., and Clukey, E.C., 2015. Seabed stiffness model for steel catenary risers. Proceedings, 3rd International Symposium on Frontiers in Offshore Geotechnics (ISFOF), Oslo, June.

Bhattacharyya, A., Tognarelli, M.A., Ghosh, R. Clukey, E.C. and Sun, Q., 2011. Simulation of SR behavior at touchdown zone–part I: numerical analysis of global SCR model vs. sectional SCR model. Proceedings, Offshore Technology Conf. Brazil, Paper OTC 22557, Rio de Janeiro, Oct.

Bea, R.G., Wright, S.G., Sircar, P. and Niedoroda, A.W., 1983. Wave induced slides in South Pass Block 70, Mississippi Delta. American Society of Civil Engineers, ASCE J. of Geotechnical Engineering, Vol. 109, No. 4, April, pp. 619-644.

Bea, R.G. 1984. Dynamic response of marine foundations. Keynote paper, Ocean Structural Dynamics Symposium '84, Corvallis, Oregon.

Bennett, R.H., 1977. Pore pressure measurements: Mississippi delta submarine sediments. Marine Geotechnology, Vol. 2, pp. 177-189.

Bennett, R.H. and Faris, R.J., 1979. Ambient and dynamic pore pressures in fine grained sediments. Applied Ocean Research, Vol 1, No. 3, pp 115-123.

Berger, W.J., Lanier, D.L. and Jeanjean. P., 2006. Geological setting of Mad Dog mooring system. Proceedings, 38th Offshore Technology Conf., Houston, Paper OTC 17914, Houston, May.

Bjerrum, L., 1973. Geotechnical problems involved in foundations of structures in the North Sea. Geotechnique, Vol. 23, No. 3 Sept. pp. 319-358.

Bridge, C., Laver, K., Clukey, E., Evans, T., 2004. Steel catenary riser touchdown point vertical interaction models. Proceedings, 36th Offshore Technology Conf., Houston, Paper OTC 16628, Houston, May.

Bridge, C.D., 2005. Effects of seabed interaction on steel catenary risers," Ph.D. Dissertation, Surrey University, December.

Bridge, C.D. and Howells, H.A., 2007. Observations and modeling of steel catenary riser trenches. Proceedings, 17th International Offshore and Polar Engineering Conference, Lisbon, ISOPE-2007-468.

Bruton, D.A.S., White, D.J., Langford, T. and Hill, A.J., 2009. Techniques for the assessment of pipe-soil interaction forces for future offshore developments. Proceedings, Offshore Technology Conf., Paper OTC 20096, Houston, May

Buckingham, E., 1914. On physically similar systems: illustrating the use of dimensional analysis. *Phys Rev*. 4: PP345-376.

Byrne, B.W. and Houlsby, G.T., 2002. Experimental investigations of response of suction caissons to transient vertical loading. American Society of Civil Engineers, ASCE J. of Geotechnical and Geoenvironmental Engineering, Vol. 128, No. 11, Nov., pp. 926-939.

CAPFOS Inc., 2013. Capacity analysis program. www.capfos.com.

Chen, W. and Randolph, M.F., 2005. Centrifuge tests on axial capacity of suction caissons in clay. Proceedings, 1st Intl. Symposium on Frontiers in Offshore Geotechnics, ISFOG, Perth, Australia, Sept., pp. 243-250.

Chen J-Y., Litton, R., Ku, A., Fraser, R., and Jeanjean, P., 2016. Seismic soil-structure interaction design considerations for offshore platforms. Proceedings, 35th Intl, Conf. on Ocean, Offshore, and Arctic Engineering, ASME, OMAE2016-54934, Busan, South Korea, June.

Clukey, E.C., 1983. Laboratory and field investigation of wave-sediment interaction. PhD dissertation, Cornell University, Ithaca, NY, 382 p.

Clukey, E.C., Kulhawy, F.H., and Liu, P.L-F., 1983. Response of silts to wave loads. Strength Testing of Marine Sediments, Laboratory and In-Situ Measurements, ASTM STP 883, Philadelphia pp. 381-396.

Clukey, E.C., Jackson, C.R., Vermersch, J.A., Koch, S.P. and Lamb, W.C., 1989. Natural densification by wave action of sand surrounding a buried offshore pipeline. Proceedings, 21st Offshore Technology Conf., Paper OTC 6151, Houston, May, pp. 291-300.

Clukey, E.C. and Morrison, M.J., 1993. A centrifuge and analytical study to evaluate suction caissons for TLP applications in the Gulf of Mexico. American Society of Civil Engineers, ASCE Geotechnical Special Publication No. 38, Dallas, pp.141-156.

Clukey, E.C., Morrison, M.J., Garnier, J. and Corte, J.F., 1995. The response of suction caissons in normally consolidated clays to cyclic TLP loading conditions. Proceedings 27th Offshore Technology. Conf., Paper OTC 7796, Houston, May, pp. 909-918.

Clukey, E.C. and Phillips, R., 2002. Centrifuge model tests to verify suction caisson capacities for taut and semi-taut legged mooring systems. Proceedings, Deep Offshore Technology Conf., New Orleans.

Clukey, E.C., Aubeny, C.P. and Murff, J.D., 2003. Comparison of analytical centrifuge model tests for suction caissons subjected to combined loads. Proceedings, 22nd Intl Conf. on Offshore Mechanics and Arctic Engineering, OMAE2003-3750, Cancun, June.

Clukey, E.C., Templeton, J.S., Randolph, M.R., and Phillips, R., 2004. Suction caisson response under sustained loads, Proceedings, 36 h Offshore Tech. Conf., Paper OTC 16843, Houston, May, pp. 909-918.

Clukey, E.C., Haustermans, L., and Dyvik, R., 2005. Model tests to simulate riser-soil interaction in touchdown point region. Proceedings, Intl. Symposium of Foundations and Offshore Geotechnics (ISFOG), Perth, Sept.

Clukey, E.C., Tognarelli M.A., Li, G., Ghosh R., Phillips R., Zakeri A., Elliot B.J., Bhattacharyya A., and Sun Q., 2011. Simulation of SCR behavior at touchdown zone-part II: testing of a sectional SCR model in a geotechnical centrifuge. Proceedings, Offshore tech. Conf. Brazil, OTC 22569, Rio de Janeiro, Oct.

Clukey E.C., Gilbert, R.G., Andersen, K.H., and Dahlberg, R., 2013. Reliability of suction caissons for deep water floating facilities. American Society of Civil Engineers, ASCE Geotechnical Special Publication No. 229, Foundation Engineering in the Face of Uncertainty, pp 456-474.

Clukey, E.C., Aubeny, C.P., Zakeri, A., Randolph, M.F., Sharma, P.P., White, D.J. and Sancio, R., 2017. A perspective of the state of knowledge regarding soil-pipe interaction for SCR fatigue assessments. Proceedings, 48th Offshore Technology Conference, Paper OTC 27564-MS, Houston, May.

Clukey, E.C. and Zakeri, A., 2017. Recent advances in nonlinear soil models for fatigue evaluation of steel catenary risers. Proceedings, 48th Offshore Technology Conf., Paper OTC 27627-MS, Houston, May.

Cross, R.H., Huntsman, S.R., Treadwell, D.D. and Baker V. A., 1979. Attenuation of pore water pressure in sand. Proceedings, ASCE Specialty Conference on Civil Engineering in the Oceans IV, Vol 2, San Francisco, pp. 745-757.

Dalrymple, R.W., 1979. Wave-induced liquefaction: modern example from the Bay of Fundy. Sedimentology, 26, pp 835-844.

DeGroot, M.B. and Meijers, P., 1992. Liquefaction of trench fill around a pipeline in the seabed. Proceedings, 6th Intl. Conf. on Behavior of Offshore Structures, Vol. 1, London.

Dickenson, S.E., 1994. Dynamic response of soft and deep cohesive soils during Loma Prieta Earthquake of October 17, 1989. Ph.D. Dissertation, University of California, Berkeley.

Doyle, E.H., 1973. Soil-wave tank studies of marine soil instability. Proceedings, 5th Offshore Technology Conf., Vol. 3, Paper OTC 1901, Houston, May, pp 753-766.

El-Sherbiny, R., 2005. Performance of suction caisson anchors in normally consolidated clays. PhD dissertation, University of Texas, Austin, August, 332 p.

Elliott, B.J., Zakeri, A., Macneill, A., Phillips, R., Li, G., and Clukey, E.C., 2013. Centrifuge modeling of steel catenary risers at TDZ, part I: development of novel centrifuge experimental apparatus. Ocean Engineering, 60.

Garnier, J., Gaudin, C., Springman, S.M., Culligan, P.J. Goodings, D., Konig, D, Kutter, B., Phillips, R. Randolph, M.F. and Thorel, L., 2007. Catalogue of scaling laws and similitude questions in centrifuge modelling. Intern. J. of Phys. Mod. In Geotech., 7(3) pp 1-24.

Gaudin, C., Clukey, E.C., Garnier, J. and Phillips, R., 2010. New frontiers for centrifuge modelling in offshore geotechnics. Proceedings, Intl. Symposium of Foundations and Offshore Geotechnics (ISFOG), Perth, November.

Grant, R.G., Litton, R.W. and Mamidipudi, P., 1999. Highly compliant rigid (HCR) riser model tests and analysis. Proceedings, 31st Offshore Technology Conf., Paper OTC 10973, Houston, May.

Grant, R.G., Litton, R.W., Finn, L., Maher, J., and Lambrakos, K., 2000. Highly compliant rigid risers: field test benchmarking a time domain VIV algorithm. Proceedings, 32nd Offshore Technology Conf., Paper OTC 11995, Houston, May.

Henkel, D.J., 1970. The role of waves in causing submarine landslides. Geotechnique, Vol. 20, No. 1, March, pp. 75-80.

House, A.R. and Randolph, M.F., 2001. Installation and pull-out capacity of stiffened suction caissons in cohesive sediments. Proceedings, 11th Intl. Offshore and Polar Engr. Conf., ISOPE, Stavenger, Norway, 2, pp. 574-580.

House, A., 2002. Suction caisson foundations for buoyant offshore facilities, PhD Dissertation, Univ. of Western Australia, Perth.

Houlsby, G.T., Kelly, R.B., Huxtable, J. and Byrne, B.W., 2006. Field trials of suction caissons in sand for offshore wind turbine foundations. Geotechnique, Vol 56. No 1, pp. 3-10.

Idriss, I.M., Dobry, R., Doyle, E.H., and Singh, R.D., 1976. Behavior of soft clays under earthquake loading conditions. Proceedings, 8th Offshore Tech. Conf., Paper OTC 2671, Houston, May.

ISO/DIS 19901-4, 2011. Petroleum and natural gas industries – special requirements for offshore structures – part 4: Geotechnical and foundation design considerations, 187 p.

Jeanjean, P., 2006. Set-up characteristics of suction anchors for soft Gulf of Mexico clays: experience from field installation and retrieval. Proceedings, Offshore. Technology. Conf., Houston, Paper OTC 18005, Houston, May.

Jeanjean, P., Znidarcic, D., Phillips, R., Ko, H-Y., Pfister, S., Cinicioglu, O., and Schroeder, K., 2006. Centrifuge testing on suction caissons: double wall, overconsolidated clay, and layered soil profile. Proceedings, 38th Offshore Technology Conf., Paper OTC 18007, Houston, May.

Jeanjean, P., 2009. Re-assessment of P-Y curves for soft clays from centrifuge testing and finite element analyses. Proceedings, 39 h Offshore Technology Conf., Paper OTC 19219, Houston, May.

Jeanjean, P., Zhang, Y, Zakeri, A, Andersen, KH, Gilbert, R, and Senanayake, AIMJ. 2017. A framework for monotonic p-y curves in clays. Proceedings, Society for Underwater Technology, 8th International Conference on Offshore Site Investigation and Geotechnics, London, September

Keaveny, J.M., Hansen, J.B., Madshus, C. and Dyvik, R., 1994. Horizontal capacity of large-scale model anchors. Proceedings, XIII ICSMFE, New Dehli, Vol. 2 pp. 677-680.

Kelly, R.B., Houlsby, G.T. and Bryne, B.W., 2006. A comparison of field and laboratory tests of caisson foundations in sand and clay. Geotechnique, Vol. 56, No. 9, pp. 617-626.

Lee, K.L. and Focht, J.A., Jr., 1975. Liquefaction potential at Ekofisk Tank in North Sea. American Society of Civil Engineers, ASCE J. of the Geotechnical Engineering, Vol. 101, No. GT1, Jan., pp. 1-18.

LeBlanc, C., Houlsby, G.T. and Byrne B.W., 2010. Response of stiff pile in sand to long term cyclic loading. Geotechnique, Vol 60, No 1, No. 2 pp. 79-90.

Lindenberg, J., Swart, J.H., Kanter, C.J. and den Boer, K., 1982. 'Wave induced pressures underneath a caisson: a compaison between theory and large scale experimants. Proceedings, 3rd Intl. Conf. on Behavior of Offshore Structures, Vol. 1, Cambridge , MA, pp. 337-357.

Litton, R.W., Chen, J-Y., Stringer, M.E., Kuttter, B.L. and Clukey, E.C., 2014. Centrifuge study of offshore platform response to earthquake excitations. Proceedings, 45th Offshore Tecchnology Conf., Paper OTC 25206, Houston, May.

Liu, P.L.-F., 1973. Damping of water waves over a porous bed. American Society of Civil Engineers, ASCE J. of the Hydraulics, Vol. 99, No. HY12, Dec., pp. 2263-2271.

Loudon, A.G., 1952. The computation of permeability from simple soil tests. Geotechnique, Vol. 3, No. 4, Dec. pp. 165-183.

Madsen, O.S., 1978. Wave induced pore pressures and effective stresses in a porous bed. Geotechnique, Vol. 28, No. 4, Dec., pp. 377-393.

McDougall, W.G., Sollitt, C.K., Vinson, T.S. and Bell, J.R., 1981. Ocean wave geotextile interaction. SEA Grant Report on Grant No. NA79AA-D-00106, Oregon State University, Corvallis, OR, 143 p.

Mitchell, J.K., 1993. Fundamentals of soil behavior,' John Wiley and Sons Inc., 437 p.

Morrison, M.J., Clukey E.C. and Garnier, J., 1994. Behavior of suction caissons under static uplift loading. Proceedings, International Conf. Centrifuge 94, Singapore, Aug.- Sept.

Murff, J.D. and Hamilton, J.M., 1993. P-ulltimate for undrained analysis of laterally loaded piles. American Society of Civil Engineers, ASCE J. Geotechnical Engineering, Vol. 119 (1) Jan., pp. 91-107.

Murff, J.D., 1996. The geotechnical in offshore engineering. Proceedings, 27th Offshore Technology Conf., Paper OTC 8265, Houston, May.

Narbitz, C.B., Parker, G., Elverhøi, A., Marr, J.G., Mohrig, D., and Harff, P.A., 2003. Hydroplaning of subaqeous debris flows and glide blocks: analytical solutions and siscussion. *J. of Geophysical Research*, Vol. 108, No. B7, 2349.

Nielsen, S.D., Isben, L.B. and Nielsen, B.N., 2017. Transiently loaded bucket foundations in saturated dense sand- demonstration of boot effect. Geotechnical Testing Journal, Vol 40, No. 6, Nov., pp. 1101-1114.

Physical Modeling in Geotechnics, 2104. Proceeding, 8th International Conf. on Physical Modeling in Geotechnics, edited by Christophe Gaudin and David White, Perth.

Randolph, M.F. and Quiggin, P., 2009. Non-linear hysteretic seabed model for catenary pipeline contact. Proceedings, 28th Conf. Offshore Mechanics and Arctic Engr., OMAE, OMAE2009-7925, Honolulu, June.

Randolph, M.F. and White, D.J., 2012. Interaction forces between pipelines and submarine slides — a geotechnical viewpoint. Ocean Engineering, 48, pp. 32-37.

Randolph, M.F. Bhat, S., Jain, S. and Mekha, B.B., 2013. Modeling the TDZ Trench and its impact on SCR fatigue life. Proceedings, 44th Offshore Technology Conf., Paper OTC 23975, Houston, May.

SAFEBUCK 2015. Safe design of pipelines with lateral buckling. Design Guideline Document 5087471/C 15 January, Atkins.

Sassa, S. and Sekiguchi, H., 1999. 'Wave-induced liquefaction of sand in a centrifuge. Geotechnique, Vol. 48, No. 5, pp. 621-638.

Scott, R.F. and Zuckerman, K.A., 1970. Study of slope instability in the ocean floor. Naval Civil Engineering Laboratory, Report No. CR-70.007, March.

Shiri, H. and Randolph, M.F., 2010. The influence of seabed response on fatigue performance of steel catenary risers in TDZ. Proceedings, Intl. Conf. Ocean, Offshore and Arctic Engineering (OMAE), OMAE2010-21153, Shanghai.

Silvestri, V., Soulie, M., Marche, C. and Louche, D., 1985. Some contributions to the wave induced listability of the seafloor. Proceedings, Offshore Mech. and Arctic Engineering Conf., Dallas, Feb.

SINTEF (2001) 'CARISIMA JIP: catenary riser/soil interaction for global rise analysis (CARISIMA),' SINTEF.

Sleath, J.F.A., 1970. Wave induced pore pressures in beds of sand. American Society of Civil Engineers, ASCE J. of the Hydraulic, Vol 96, No. HY2, Jan. pp. 367-378.

Templeton, J.S. III, 2002. The role of finite elements in suction caisson design analysis. Proceedings, 33rd Offshore Tech. Conf., Paper OTC 14235, Houston, May.

Templeton, J.S. III, 2012. Finite element analysis in offshore geotechnics – 1 thirty-year perspective. SIMULIA Customer Conference, 19 p.

Templeton, J.S. III, 2019. Jack-up spud can foundation fixity for various clay strength profiles. Proceedings, 24th Offshore Symposium, Texas Section of the Society of Naval Architects and Marine Engineers (SNAME), Houston, Feb.

Tsui, Y. and Helfrich, S.C., 1983. Wave induced pressures in submerged sand layer. American Society of Civil Engineers, ASCE J. of the Geotechnical Engineering, Vol. 109, No. 4, April, pp. 603-618.

Vukovich, F.M., Crissman, B.W., Bushnell, M., and King, W.J., 1979. Some aspects of the oceanography in the Gulf of Mexico using satellite and in-situ data. J. Geophysical Res., 84, pp. 7749-7768.

White, D.J. Take, W.A., Bolton, M.D., 2003. Soil deformation measurement using particle image velocimetry (PIV) and photogrammetry. Geotechnique, 53(7) pp 619-631.

White, D.J., Randolph, M.F., and Thompson, B., 2005. An image-based deformation measurement system for the geotechnical centrifuge. Intl. J. of Physical Modelling in Geotechnics, 5(3), pp. 1-12.

White, D., Clukey, E.C., Randolph, M.F., Boylan, N.P., Bransby, M.F., Zakeri, A. and Hill, A.J., 2017. The state of knowledge of pipe-soil interaction for on-bottom pipeline design. Proceedings, 48th Offshore Technology Conf., Paper OTC 27623-MS, Houston, May.

Willis, N.R.T. and West, P.T.J., 2001. Interaction between deepwater catenary risers and a soft seabed: large scale sea trials. Proceedings, 33rd Offshore Technology Conf., Houston, May.

Wright, S.G., and Dunham, R.S., 1972. Bottom stability under wave-induced loading. Proceedings, 4th Offshore Technology Conf. Vol. 1, Houston, May, pp. 853-862.

Yamamoto, T., 1978. Seabed instability from waves. Proceedings, 10th Offshore Technology Conf. Vol. 1, Houston, May, pp. 1819 -1828.

Yamamoto, T., Koning, H.L., Sellmeijer, H. and van Hijum, E., 1978. On the response of a poro-elastic bed to waterwaves. J. of Fluid Mechanics, Vol. 87, No. 1, pp. 193-206.

Yuan, F., White, D. W., and O'loughlin, S. D., 2016. The evolution of seabed stiffness duringcyclic movement in a riser touchdown zoneon sift clay, Geotechnique, July10.1680jgeot.15.P.161

Zakeri, A., Hoeg, K. and Nadim F., 2008. Submarine debris flow impact on pipelines – part I: experimental investigation. Coastal Engineering, 55, pp. 1200-1218.

Zakeri, A., 2008. Submarine debris flow impact on pipelines: drag forces, mitigation and control. Proceedings, 39th Offshore Technology Conf., Paper OTC 19173, Houston, May.

Zakeri, A., 2009. Submarine debris flow impact on suspended (free apan) pipelines: normal and longitudinal drag forces. Ocean Engineering, 36, pp. 489-499.

Zakeri, A., 2012. Drag forces caused by submarine glide block or out-runner block impact on suspended (free-span) pipelines. Ocean Engineering, 47, pp. 50-57.

Zakeri, A., Clukey, E., Kebadze, B., Jeanjean, P. Piercey, J., Templeton, J. Connelly, L., and Aubeny, C., 2015. Recent advances in soil response modeling for well conductor fatigue analysis and development of new approaches. Proceedings, 46th Offshore Technology Conference, Paper OTC 25795-MS, Houston, May.

Zeevaert, L., 1958. Liquefaction of fine sand due to wave action. Proceedings, 6th Conf. Coastal Engineering, Chapter 49, pp. 818-826.

Zheng, B.L., Kutter, B.L., Hirt, G.S., Zhou, Y.G., Wilson, D.W. and Clukey, E.C., 2015. Centrifuge modeling of seismic behavior of caisson-supported subsea manifold on soft clay. Proceedings, 6th Intl Conf. Earthquake & Geotechnical Engineering, (6ICEGE), Christchurch, New Zealand, November.